J Appl Electrochem (2012) 42:645–666
DOI 10.1007/s10800-012-0457-6

ORIGINAL PAPER

Macrohomogeneous approach to a two-dimensional mathematical model of an industrial-scale electrodialysis unit

Roman Kodým · Petr Pánek · Dalimil Šnita · David Tvrzník · Karel Bouzek

Received: 31 May 2012 / Accepted: 14 July 2012 / Published online: 11 August 2012

Abstract In this manuscript a novel way of mathematical modelling of the electrodialysis process, based on a macrohomogeneous approach, is introduced. It enables an industrial-scale unit to be described without unrealistic simplifications, thus providing information about the local distribution of various physical quantities inside this apparatus based on the operational parameters studied. The two-dimensional model presented takes into consideration a spatial variation of the effective flow cross-sectional area of the geometry of a real electrodialysis unit. The key feature of this macrohomogeneous model is the anisotropy of individual macrohomogeneous domains described by corresponding balance and transport partial differential equations. A classical Nernst–Planck model is used to describe NaCl transport inside the unit. The proposed model approach is experimentally validated for a medium degree of water desalination (up to 40 %). By means of this model the principal consequences of the non-uniform hydrodynamics in the electrodialysis unit are demonstrated. It is shown that non-uniform distribution of diluate in the individual diluate compartments results in (a) a significant decrease in overall process efficiency due to an increase in the value of parasitic current and (b) a concentration of the electric current in a narrow area. The latter aspect, in combination with locally lowered linear velocity of the solution, may lead to an enormous increase in temperature and subsequent deterioration of the membranes. Such a situation is, therefore, highly dangerous from the point of view of process reliability.

Keywords Electrodialysis · Water desalination · Industrial-scale · Macrohomogeneous mathematical model · Plate-and-frame design

R. Kodým · P. Pánek · K. Bouzek (✉)
Department of Inorganic Technology, Institute of Chemical Technology Prague, Technická 5, 166 28 Prague 6, Czech Republic
e-mail: bouzekk@vscht.cz

D. Šnita
Department of Chemical Engineering, Institute of Chemical Technology Prague, Technická 5, 166 28 Prague 6, Czech Republic

D. Tvrzník
MemBrain s.r.o., Pod Vinicí 87, 471 27 Stráž pod Ralskem, Czech Republic

List of symbols

Variables

a	Cross-section area fraction
B	Darcy's coefficient analytically derived for a channel enclosed in-between two parallel plates and under laminar flow conditions ($m^2\ Pa^{-1}\ s^{-1}$)
c	Molar concentration of NaCl (mol m^{-3})
d	Depth (m)
$\mathbf{D}$	Tensor of anisotropic binary diffusion coefficients of NaCl ($m^2\ s^{-1}$)
$D_{i,x}\ D_{i,y}$	Binary diffusion coefficient of NaCl in x and y directions ($m^2\ s^{-1}$)
F	Faraday constant (C mol^{-1})
f	Volumetric fraction
$\mathbf{G}$	Tensor of anisotropic specific conductivity (S m^{-1})
$G_{i,x}\ G_{i,y}$	Overall specific conductivity of the system in x and y directions (S m^{-1})
GDD	Global degree of desalination (%)
h	Thickness, height (m)
$\hbar$	Relative thickness
I	Electric current (A)

j	Current density (A m^{-2})
J	Molar flux density of NaCl (mol m^{-2} s^{-1})
l	Length (m)
n	Dimensionless unit vector normal to the boundary
N	Source/sink term of NaCl (mol m^{-3} s^{-1})
p	Pressure (Pa)
P	Tensor of anisotropic hydraulic permeability (m^2 Pa^{-1} s^{-1})
$P_{i,x}$ $P_{i,y}$	Hydraulic permeability of the system in x and y directions (m^2 Pa^{-1} s^{-1})
Q	Volumetric flow rate (m^3 s^{-1})
R	Universal gas constant (J K^{-1} mol^{-1})
S	Cross-sectional area (m^2)
T	Temperature (K)
U	Total voltage (V)
U_M	Membrane potential (V)
U_p	Voltage drop in one membrane pair (V)
v	Solution flow velocity (m s^{-1})
v^*	Linear velocity in the individual working chambers (m s^{-1})
$\bar{v}$	Average linear velocity in the working chambers (m s^{-1})

Greek symbols

β	Electroosmotic coefficient (m^2 A^{-1} s^{-1})
ϕ	Galvani potential (V)
η	Dynamic viscosity (Pa s)
κ_R	Dimensionless empirical constant used to correct the resistance of the membrane stack in the y direction
κ_B	Dimensionless empirical constant used to correct the analytically derived value of Darcy's coefficient B
κ_H	Dimensionless empirical constant used to correct the hydraulic resistance of the membrane stack
κ_{15y}	Dimensionless permeability coefficient used to vary the overall permeability of the feed and drain channels along the membrane stack (i.e. in the y direction)
μ	Overall solute permeability across membranes (s^{-1})
π	Solvent permeation coefficient (m^3 mol^{-1} s^{-1})
σ	Free-volume specific conductivity (S m^{-1})
ψ	Overall current efficiency

Subscripts

(1)…(19)	Numbering of boundaries
AM	Anion-selective membrane
CM	Cation-selective membrane
C	Concentrate stream or solution
D	Diluate stream or solution
DC	Distribution channels
i	Subdomain number
in	Inlet
j	Layer of a membrane pair
M	Membrane
OCC	Outlet collecting channels
out	Outlet
p	Membrane pair
rel	Relative

Abbreviations

1D, 2D, 3D	One-, two- and three-dimensional
AM	Anion-selective membrane
CM	Cation-selective membrane
CC	Concentrate compartment
C	Concentrate stream
DC	Diluate compartment
D	Diluate stream
ED	Electrodialysis
SMP	Single membrane pair

1 Introduction

Electrodialysis (ED) ranks among the industrial, electromembrane separation processes. Especially in the field of brackish water desalination, which represents the most widespread use of this technology, ED is nowadays in competition with the conventional reverse osmosis process [1–7]. There is also an increasing trend to apply ED in waste water recovery and desalination of process streams in the pharmaceutical and food industries. The advantage of the electromembrane separation process is that it does not endanger health or the nutritious properties of the final product, e.g. by adding coagulants or regenerating agents. The demineralization of milk whey is a representative example [8].

The core of an electrodialyzer of the plate-and-frame filter-press type is the membrane stack, consisting of alternated planar anion-selective (AM) and cation-selective (CM) membranes. The individual membranes are separated by electrochemically inactive spacers serving mainly as a mechanical support of the stack and determining the space for the flow of the process solutions in-between the membranes. Generally, two independent hydraulic circuits are considered in the model, i.e. the diluate stream (D) and the concentrate stream (C), supplying diluate and concentrate solutions to the diluate (DC) and concentrate compartments (CC). A set of one AM and one CM with corresponding compartments (DC and CC) is a repeated component of the ED unit often denoted as a membrane pair. For more details, an expanded scheme of the ED unit is illustrated in Fig. 1. Besides the two hydraulic circuits discussed, an auxiliary hydraulic circuit is used to wash the electrode compartments. Since they have no direct influence on the flow hydrodynamics and electric potential field distribution inside the ED stack, they are not considered in the present model and are therefore, not discussed in this paper. The driving force of the separation process is the

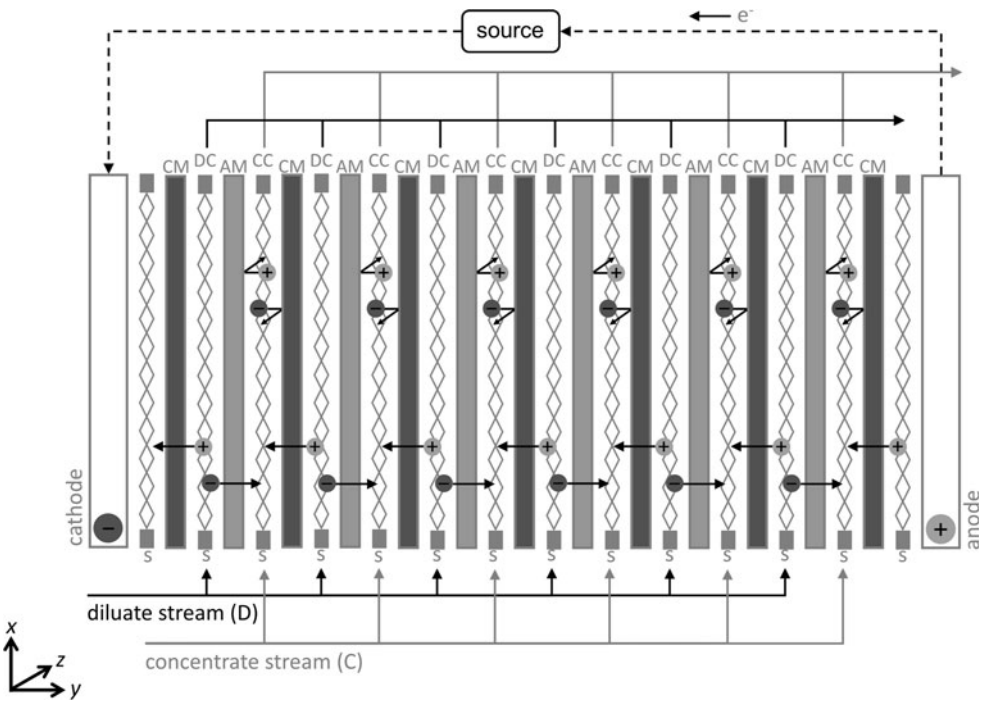

Fig. 1 Schematic of the electrodialyzer and electrodialysis process. *D* diluate stream, *C* concentrate stream, *S* net-like spacer, *DC and CC* diluate and concentrate compartments, *AM and CM* anion- and cation-selective membranes, (+) cations, (−) anions; adopted coordination system: *x*-coordinate—direction of the main flow of the solution in the diluate and concentrate compartments, *y*-coordinate—direction perpendicular to the membrane surface

electric field imposed on the membrane stack between two terminal electrodes. The basic principles of this process are summarized in the literature [1–4, 9].

Currently, one of the main development paths of ED units is to increase its capacity. This is motivated by the need to significantly reduce the capital and operating costs per unit of treated solution. Such scale-up can be achieved, for example, by increasing the number of membrane pairs in the stack and/or by increasing the active area of the membrane. However, these modifications bring about new problems, connected not only with the mechanical stability of the ED unit, but also with the uniformity of the charge and mass fluxes inside the system. For example, by increasing the number of membrane pairs, the danger of inhomogeneous solution distribution between the individual diluate compartments increases significantly. At the same time, the cell voltage, i.e. the driving force of parasitic (shortcut, bypass) current via the feed and drain channels [10], also increases.

This problem is theoretically similar to the existence of parasitic current in an electrolyzer with a bipolar electrode arrangement, as discussed in detail, for example, in [11, 12]. Furthermore, inhomogeneous hydrodynamics in the inter-membrane space may lead to locally enhanced solution desalination and reduced process efficiency due to concentration polarization. In an extreme case, it may lead to local membrane deterioration due to the enhanced electric field [13] or locally concentrated electric current. These effects are further intensified in the diluate compartment characterized by notably lower linear velocity compared to the remaining compartments of the membrane stack. This typically occurs in the case of non-uniform distribution of process solution in the diluate compartments along the membrane stack. Up to now complications connected with non-uniform mass and charge fluxes have solely been solved empirically. Such an approach is, however, no longer viable due to the related high costs and time demands associated with the development and optimization of industrial ED units, especially in the case of the large units designed recently. From this point of view mathematical modelling is considered to be a promising and effective complementary approach to the experimental one.

Mathematical modelling is already well established in the field of ED process optimization. However, so far the main focus has been on the individual parts of the entire system. There is still a significant lack of theoretical studies targeting a mathematical description of an entire ED unit capable of predicting the local distribution of mass and charge fluxes in this system. The main reason is that such models have to be two- (2D) or three-dimensional (3D) and have to take a large number of membrane pairs into account. They thus make enormous demands on the computational power of the hardware. This fact is especially relevant in the case of the mathematical modelling of industrial-scale apparatus. A number of model restrictions of the physical reality have to be adopted to reduce the demands made of models to an acceptable level, for instance, the conversion of the system dimensions to a 2D or 1D model of one membrane pair. Most commonly the Nernst–Planck equation is used to describe the ion transport in the model system and ideally permselective membranes are considered. Concentration polarization effects are often integrated into the models by means of the experimentally determined limiting current density of the AM and

CM to describe the system's behaviour at high current densities. However, it is difficult to determine the thickness of the laminar boundary layer and the Nernst diffusion layer at the membrane surface. Their values vary significantly with the position and depend on a vast number of parameters, especially the geometry of the flow channel and the net-like spacer [14]. Thus, the application of such a concept is questionable. Physical phenomena, playing an important role at high current density close to or exceeding the limiting current densities, are often neglected because they take place on a local scale near the membrane surface; to take them into consideration would significantly increase the complexity and computational demands of the model. These phenomena are thoroughly reviewed in the paper of Nikonenko et al. [15].

The predominant number of mathematical modelling studies on the ED process has so far been confined to a description of the hydrodynamics in the channel between the membranes. Practically applicable mathematical models enabling a characterization of the liquid flow in an industrial-scale membrane channel have been presented, for instance, by Dirkse et al. [16], Kostoglou and Karabelas [17] and Kodým et al. [18]. These models are 2D to provide acceptable computational demands and to describe the solution flow in the plane parallel to the membrane surface. Dirkse et al. [16] applied a potential flow theory, which accurately described the distribution of the process solution in the intermembrane space without an inserted spacer net. However, the spacer net represents an integral part of electrodialysis, thus to neglect it represents an unacceptable simplification of reality. The effect of the net-like spacer was later introduced by Kostoglou and Karabelas [17]. The channel filled by the spacer net was simulated as a continuous phase characterized by the anisotropic permeability tensor as a function of the net structure and macroscopic flow velocity. This means that inertial forces were also taken into account in the momentum balance. The permeability tensor was determined by the direct solution of the Navier–Stokes equation on a single "unit cell". The mathematical model proposed in this work is highly efficient and straightforward. Nevertheless, it does not describe the 3D character of the flow typical of a channel with net-like spacers. This problem was partially solved by a model approach proposed by Kodým et al. [18]. Here, the flow channel was divided into two 2D hydraulic layers. The flow direction in each of them was determined by the direction of the spacer filaments' orientation. For simplification purposes a viscous flow regime was considered. The significant importance of the inertial forces acting on the moving liquid was recently demonstrated by Pánek et al. [19]. However, a consideration of the inertial forces tremendously increases the demands of the model on the computational power of the hardware.

A few remaining studies are only concerned with the distribution of the electric current in the electrodialyzer by means of an equivalent circuit approach and assuming uniform mass distribution and constant properties of the system [10, 20]. Mandersloot and Hicks [20] showed that the electrical current flows continuously from the diluate and concentrate compartments to the feed and drain channels along the entire membrane stack and not only in the narrow region close to the electrodes. Similar results were obtained by Veerman et al. [10], who employed an equivalent circuit model to calculate parasitic current in a reverse ED unit. Their model predicted membrane stack resistance twice lower than the experimental observations. This deviation may stem from (i) strong concentration-dependent behaviour of the membranes, (ii) restricted ion transport in the spacers, (iii) neglected concentration polarization and (iv) a shadow effect from the spacer net on the membranes.

Combining the mass and charge balances to fully describe the ED process further increases the complexity of the final model. The model system is frequently reduced to a 2D or 1D mathematical model of one membrane pair. A 2D model of one membrane pair in the cross-section normal to the membrane surface and parallel to the direction of the main solution flow was, for example, solved analytically by Shaposhnik et al. [21] who demonstrated the relationship between the operational parameters and thickness of the diffusion layer in dependence on the position along the solution flow coordinate. The model agreed with the experimental data up to a current load of around 80 % of limiting current density. The discrepancies at higher current densities were explained by side effects like water dissociation, co-ion backward diffusion from the concentrate compartment to the diluate stream, electro-osmotic transfer, violation of the electroneutrality condition, etc., neglected in the model.

This single membrane pair (SMP) approach is often employed to describe the behaviour of the entire ED unit based on the assumption of the system periodicity [22–24]. A 1D analytical model of an ED unit using this approach was proposed by Lee et al. [22] and it was even applied for optimization of a desalting plant. Later, Brauns et al. [23] investigated the experimental verification of the solver software for the design and configuration of an ED unit, based on a mathematical model analogous to that of Lee. Furthermore, Veerman et al. [24] presented a theoretical analysis of the possibility of electrode segmentation in the reverse electrodialysis process by means of a 1D SMP model. It was demonstrated both by the mathematical model and experimentally that the electrode segmentation may result in an increase of up to 15 % of power output compared to a unit configuration with compact electrodes.

It is clear that the classical SMP model represents an effective tool for ED process optimization. However, it does not take into account the effect of hydrodynamic non-uniformity in the ED unit. The variation of the linear

velocity in the diluate channels along the membrane stack occurs, for example, due to construction irregularities and due to pressure variation in the feed and drain channels. Because of the former effect it is hard to predict the velocity distribution. This factor was statistically treated and taken into account by Tanaka [9, 25–27] who postulated that the frequency distribution of the velocity ratio $\xi = \frac{v^* - \bar{v}}{\bar{v}}$ (v^* and $\bar{v}$—local and average linear velocity in DC and CC) obeys normal distribution characterized by a certain standard deviation. It was demonstrated experimentally and by mathematical modelling that standard deviation has to be below 0.2. This was integrated into the SMP model by means of the limiting current density of the electrodialyzer. This is, in fact, the limiting current density of the CM at the outlet of the diluate compartment with the lowest linear velocity. This limiting current density should not be overcome, otherwise the process efficiency would rapidly decrease.

An interesting model approach was recently presented by Pánek et al. [28]. This model is spatially 2D and it includes one membrane pair in the plane parallel with the membranes. A laminar flow hydrodynamics in the intermembrane space with a net-like spacer was considered, calculated using an external, spatially 2D model described in [18]. Mass and charge transport across the membranes were considered via migration and electro-osmosis, described by linearized Nernst–Planck's and Schlögl's equations, respectively. The results of the mathematical model indicated very significant inhomogeneities in the solution flow and in the local degrees of desalination of the solution. In this case ideally flat membranes were considered, which represents a significant simplification. As demonstrated experimentally by Tanaka [9], local deformations of the membrane significantly affect the local solution velocity in the intermembrane space. Tanaka finally emphasized the necessity to avoid membrane deformation in order to prevent flow regularities in this system.

From the above literature review it is apparent that there is currently a considerable lack of efficient numerical models enabling the calculation of the local distribution of various physical quantities inside an industrial-scale ED membrane stack in dependence on a wide range of operational parameters. The absence of such a model becomes the limiting aspect to further development of the ED process. The aim of this work is, therefore, to extend the set of available mathematical models and to provide an effective tool for ED process optimization. A novel 2D mathematical modelling concept, which fulfils these requirements, has accordingly been developed. The model is macrohomogeneous and based on conventional principles, such as mass and charge transport and the corresponding balances. The proposed model features acceptable computational demands, exhibits satisfactory accuracy and is suitable for practical engineering calculations.

2 Model system and geometry

The model ED unit under study, schematically depicted in Fig. 1, is of the typical plate-and-frame type consisting of 200 membrane pairs. The planar membranes are oriented vertically and are separated by a sheet-flow net-like spacer with a non-woven symmetric net. A schematic illustration of the sheet-flow spacer used is shown in Fig. 2A, B. It consists of five main parts. The cut-outs (1) and (5) in the spacer frame form horizontal feed and drain channels in the membrane stack. These channels supply or drain the process solutions into and from the DC and CC, respectively. The small channels (2) and (4) distribute or collect solution into or from the individual intermembrane compartments (3), respectively. The diluate and concentrate compartments (3), also called working chambers, are filled with spacer net and represent the working part of the membrane stack. Note that, except for the position of the drain and feed channels (compare Fig. 2a, b), the spacers in the DC and CC have identical geometry. The basic geometrical parameters of the ED unit under study are summarized in Table 1.

It is apparent that the ED unit is highly geometrically structured and anisotropic. This is due to the complex geometry of the net-like spacer used and the extremely high number of interfacial boundaries in the membrane stack. An accurate mathematical description of this system requires a 3D model with very fine discretization, consisting of grid elements significantly smaller than the intermembrane distance. Such a model would not, however, be feasible for industrially relevant systems; moreover, the computational time of the corresponding parametric studies would be extremely long. To decrease the computational demands of the final model, two main simplifications of the model geometry were adopted in this work.

The first one is the adoption of geometrical symmetry of the ED unit in the direction of the z-axis. This allowed a reduction of the model dimension to 2D, represented by the x–y cross-section perpendicular to the membrane surface and parallel to the direction of the main flow of the solution. The resulting 2D model geometry is depicted in Fig. 3. In this figure the membranes are oriented horizontally with the anode on the top. This orientation is applied throughout this study. The assumption of symmetry along the z-coordinate is acceptable in the subdomain of the working chamber, but its application in the subdomains of the feed and drain channels as well as the distribution and

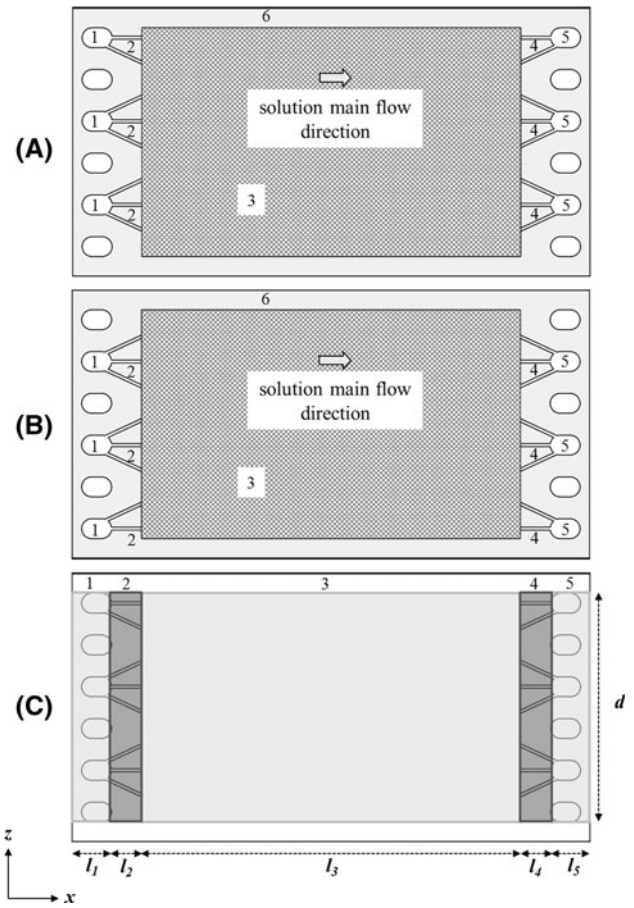

Fig. 2 **A**, **B** Schematic illustration of the used sheet-flow spacers—*top view*; spacers in the diluate and concentrate compartments are identical and differ only in the position of feed and drain channels, compare **A** for diluate and **B** for concentrate; *1* and *5* cut-outs in the spacer frame for the feed and drain channels, respectively; *2* and *4* cut-outs for the inlet distribution and outlet collecting channels, respectively; *3* DC and CC (working chamber) filled with spacer net; *6* polyethylene spacer frame. **C** Schematic illustration of the spacer segmentation in five subdomains uniform along the *z*-coordinate, original geometry is indicated below the domains on account of their localization and meaning; *1* and *5* subdomains of the feed and drain channels, respectively; *2* and *4* subdomain of the inlet distribution and outlet collecting channels, respectively; *3* subdomain of the DC and CC (working chamber); dimensions: $d = 32.0$ cm; $l_1 = l_5 = 8.7$ cm, $l_2 = l_4 = 6.8$ cm, $l_3 = 65.0$ cm

collecting channels is under question, see Fig. 2C. This is due to their real geometry with a significantly reduced active cross-section area. To preserve the effect of real geometry in the model, the system of the ED unit is divided into five subdomains uniform along the *z*-coordinate, see Figs. 2C and 3. Different effective properties are then used in the individual subdomains instead of explicitly modelled geometric details of the net-like spacer. The resulting subdomains correspond to the following parts of the ED unit: 1 and 5 represent subdomains of the feed and drain channels, respectively; 2 and 4 are subdomains of the inlet distribution and outlet collecting channels, respectively; and 5 is the working part of the membrane stack, i.e. set of DCs or CCs. The anode phase represents an additional subdomain (not numbered in Fig. 3). The electric current feeder is connected to anode boundary no. 11 and the current collector to boundary no. 9. This will be discussed in more detail in Sect. 3.4.

The second simplifying assumption stems from the fact that, in the case of the industrial ED unit with several hundred membranes, the thickness of one membrane pair is negligible compared to the dimensions of the entire membrane stack. For this reason, the distinct interfaces between membranes, spacers and solution diminish and the multi-phase system appears to be macrohomogeneous and continuous in the direction normal to the membrane surface, i.e. along the *y*-axis. On account of the absence of a high number of interfaces, the computational grid resolution can be substantially reduced and the model domain can be described by classical continuous partial differential equations (PDE) based on the principles of conservation of mass and charge. The resulting model domain then consists of three overlapping continuous layers: (i) diluate solution phase, (ii) concentrate solution phase and (iii) charge transport phase, which are interconnected via mass and charge source and sink terms in the corresponding PDE balance equations. This assumption represents the main novelty of the proposed model. If successfully validated, it can be used to describe diverse complex systems consisting of a high number of individual units.

The real model system is, however, highly anisotropic, i.e. individual effective properties are dependent on the position. This is due, for instance, to the fact that membranes are almost impermeable to liquid and thus the solution flows preferentially parallel to the membrane surface. On the contrary, electric charge flows spontaneously in every direction only in dependence on the actual conductivity of the pathway. This anisotropy is preserved in the proposed model by corresponding anisotropic effective properties of the individual subdomains.

3 Mathematical model description

To summarize, the proposed model is 2D, macrohomogeneous, anisotropic, stationary and isothermal. The proposed model concept is demonstrated for the water desalination process in the range of a medium degree of desalination. Several simplifying assumptions of the model physics were adopted:

- The real process solution containing various cations and anions is substituted by a model solution of NaCl with similar properties. The solution is considered to be ideal.

Table 1 Geometrical parameters of the model ED unit under study

Symbol	Value	Unit	Description
$l_1 = l_5$	8.7	cm	Length of subdomain 1 and 5
$l_2 = l_4$	6.8	cm	Length of subdomain 2 and 5
l_3	65.0	cm	Length of subdomain 3
d	32.0	cm	Depth of the system
h_1	54.8	cm	Height of the membrane stack
h_2	2.0	cm	Height of the auxiliary anode
N	200		Number of membrane pairs
h_p	0.274	cm	Thickness of one membrane pair
h_{AM}	0.057	cm	Thickness of AM
h_{CM}	0.057	cm	Thickness of CM
h_C	0.080	cm	Thickness of spacer in the DC
h_D	0.080	cm	Thickness of spacer in the CC
f_{net}	0.15		Volumetric fraction of spacer net

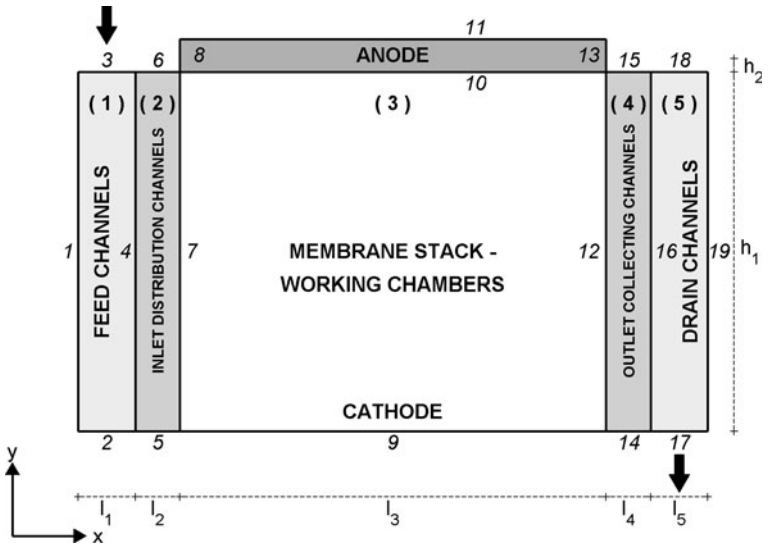

Fig. 3 Schematic of the model geometry; membranes oriented horizontally; *black arrows* indicate process solution inlet and outlet; subdomains: *1* and *5* feed and drain channels; *2* and *4* inlet distribution and outlet collecting channels; *3* working part of the membrane stack; *numbers in italic* numbering of boundaries; *bold numbers in round brackets* numbering of subdomains; dimensions: $l_1 = l_5 = 8.7$ cm, $l_2 = l_4 = 6.8$ cm, $l_3 = 65.0$ cm, $h_1 = 54.8$ cm, $h_2 = 2.0$ cm; not to scale

- Water permeation through the membranes (e.g. by water drag, osmosis or leakage) is neglected.
- The charge transport proceeds solely by transport of NaCl from the DC to the CC. The system behaves like an ohmic resistance.
- The membranes are considered to be ideally permselective for cations or anions. In consequence the concentration of co-ions in the membrane is equal to zero. The membrane specific conductivity is thus independent of the concentration of the surrounding solutions.
- The concentration gradients in the intermembrane space in the direction perpendicular to the membrane surface are neglected. This corresponds to an ideal radial mixing of the solution.

3.1 Charge balance

The charge balance is represented by Eq. (1)

$$\nabla \cdot \mathbf{j} = 0. \tag{1}$$

Here $\mathbf{j}$ represents the vector of local current density given by Eq. (2)

$$-\mathbf{G} \cdot \begin{pmatrix} \frac{\partial \phi}{\partial x} \\ \frac{\partial \phi}{\partial y} - \frac{U_M}{h_p} \end{pmatrix} = \mathbf{j}. \tag{2}$$

According to this equation, the electric charge flow is proportional to the gradient of Galvani potential ϕ. The coefficient of proportionality represents anisotropic specific conductivity included in conductivity tensor $\mathbf{G}$. The driving force of the charge flow in the direction perpendicular to

the membrane surface is reduced by the contribution of the membrane potential U_M, which is considered to be zero in subdomains 1, 2, 4 and 5. In subdomain 3 of the working chambers Eq. (3), which is derived under the assumption of ideal membrane selectivity and ideal solutions, is employed to obtain the value of the membrane potential.

$$U_M = 2\frac{RT}{F}\ln\left(\frac{c_C}{c_D}\right) \tag{3}$$

R, T and F represent the universal gas constant, temperature and Faraday constant, respectively. c_C and c_D correspond to the NaCl concentration in the concentrate and diluate solutions, respectively. The contribution of U_M is averaged with respect to the thickness of one membrane pair h_p. Generally, U_M/h_p represents the gradient of the membrane potential in the direction normal to the surface of the membrane.

The conductivity tensor $\mathbf{G}$ characterizes the anisotropic effects of the model system and is given by Expression (4).

$$\mathbf{G}(x,y) = \begin{pmatrix} G_{i,x}(x,y) & 0 \\ 0 & \kappa_R G_{i,y}(x,y) \end{pmatrix} \tag{4}$$

The individual components $G_{i,x}$ and $G_{i,y}$ represent the overall effective specific conductivities of the system in the x and y directions, respectively. They are a function of position because the specific conductivity of the process solutions σ_D and σ_C in the diluate and concentrate solutions, respectively, vary locally with NaCl concentration. Furthermore, $G_{i,x}$ and $G_{i,y}$ change stepwise between the individual subdomains i because of the complex geometry of the net-like spacer (different active cross-section areas in the individual subdomains). The values of $G_{i,x}$ are given by Eq. (5) and are described by means of the resistors connected in parallel because an ionic current flows in parallel through the CM, AM, and the diluate and concentrate solutions. $G_{1,y}$ and $G_{5,y}$ are calculated in the same manner because the prevailing ionic current flows in the direction of the y-axis in parallel through the feed and drain channels. The expression for $G_{1,y}$ and $G_{5,y}$ is given in Eq. (6). The constant κ_R introduced in Expression (4) represents a correction of the overall specific conductivity of the system in the direction of the y-axis. The meaning of this constant will be discussed in more detail in Sect. 5.1.

$$G_{i,x} = f_{i,D}\sigma_D(x,y) + f_{i,C}\sigma_C(x,y) + f_{i,CM}\sigma_{CM} + f_{i,AM}\sigma_{AM} \tag{5}$$

$$\begin{aligned} G_{1,y} &= f_{1,D}\sigma_D(x,y) + f_{1,C}\sigma_C(x,y) \\ G_{5,y} &= f_{5,D}\sigma_D(x,y) + f_{5,C}\sigma_C(x,y) \end{aligned} \tag{6}$$

By contrast, the charge in the y direction flows in subdomains 2, 3 and 4 across four layers of one membrane pair, where each layer represents an ionic conductive path connected in series to each other. The specific conductivity $G_{2,y}$, $G_{3,y}$ and $G_{4,y}$ is thus described by the resistors lined up in series. This is expressed by Eq. (7).

$$G_{i,y} = \frac{1}{\frac{\hbar_D}{a_{i,D}\sigma_D(x,y)} + \frac{\hbar_C}{a_{i,C}\sigma_C(x,y)} + \frac{\hbar_{CM}}{a_{i,CM}\sigma_{CM}} + \frac{\hbar_{AM}}{a_{i,AM}\sigma_{AM}}} \quad \text{for } i \approx 2,\ 3 \text{ and } 4 \tag{7}$$

$\hbar_j$ represents the relative thickness of the jth layer of membrane pairs ($j \approx$ AM, CM, D and C) with respect to the thickness of the membrane pair according to Eq. (8), where h_j is the thickness of the jth layer.

$$\hbar_D = \frac{h_D}{h_p}; \quad \hbar_C = \frac{h_C}{h_p}; \quad \hbar_{CM} = \frac{h_{CM}}{h_p}; \quad \hbar_{AM} = \frac{h_{AM}}{h_p} \tag{8}$$

The coefficients $f_{i,j}$ in Eqs. (5) and (6) and $a_{i,j}$ in Eq. (7) denote the volumetric and cross-sectional area fractions, respectively, of the jth ionic conductive phase in the ith subdomain. These coefficients represent a correction of the free volume specific conductivities σ_j, which stems from the simplification of the 3D net-like spacer geometry to 2D geometry symmetrical along the z-axis, as discussed above. The expressions for $f_{i,j}$ and $a_{i,j}$ are given by Eq. (9).

$$\begin{aligned}
&f_{1,D} = f_{5,D} = f_{1,C} = f_{5,C} = f_{FC} = \frac{n_{FC}S_{FC}h_p}{dl_1h_p} \\
&f_{1,CM} = f_{5,CM} = (1-2f_{FC})\hbar_{CM} \\
&f_{1,AM} = f_{5,AM} = (1-2f_{FC})\hbar_{AM} \\
&f_{2,D} = f_{4,D} = \frac{S_{DC}h_D}{dl_2h_p} \\
&f_{2,C} = f_{4,C} = \frac{S_{DC}h_C}{dl_2h_p} \\
&f_{2,CM} = f_{4,CM} = \hbar_{CM} \\
&f_{2,AM} = f_{4,AM} = \hbar_{AM} \\
&f_{3,CM} = \hbar_{CM} \\
&f_{3,AM} = \hbar_{AM} \\
&f_{3,C} = f_{3,D} = (1-f_{net})\hbar_C = (1-f_{net})\hbar_D \\
&a_{2,D} = a_{2,C} = a_{2,CM} = a_{2,AM} \\
&\quad = a_{4,D} = a_{4,C} = a_{4,CM} = a_{4,AM} = \frac{S_{DC}}{dl_2} \\
&a_{3,D} = a_{3,C} = 1 - f_{net} \\
&a_{3,CM} = a_{3,AM} = 1
\end{aligned} \tag{9}$$

Here f_{FC} denotes the volumetric fraction of the feed channels supplying either diluate or concentrate solution, S_{FC} is the cross-sectional area of one feed channel, n_{FC} represents the number of feed channels corresponding either to the diluate or the concentrate solution, and S_{DC} is the top-view area of the inlet distribution channels in the x–z plane in subdomain 2. The meaning of the symbols d, l_1 and l_2 is clear from Fig. 2c. Some coefficients $f_{i,j}$ and $a_{i,j}$ have an identical value in subdomains 1 and 5, or 2 and 4,

resulting from the symmetrical geometry of the inlet and outlet region of the net-like spacer used. Finally, f_{net} denotes the volume fraction of the net in the diluate or concentrate compartments.

σ_D and σ_C were calculated from the concentration of NaCl in the solution by means of empirical polynomial Eq. (10)

$$\begin{aligned} \sigma_i &= p_1 c_i^3 - p_2 c_i^2 + p_3 c_i \,(\mathrm{S\ m^{-1}}) \\ p_1 &= 4.608 \times 10^{-9}\,\mathrm{S\,m^8\,mol^{-3}} \\ p_2 &= 5.998 \times 10^{-6}\,\mathrm{S\ m^5\,mol^{-2}} \\ p_3 &= 11.201 \times 10^{-3}\,\mathrm{S\ m^2\,mol^{-1}}, \end{aligned} \tag{10}$$

where subscript i denotes diluate or concentrate solution. This empirical dependence was obtained by fitting experimental data obtained at a temperature of 25 °C [29].

3.2 Material balance

The material balances of NaCl in diluate and concentrate solutions are considered in the form of Eq. (11).

$$\nabla \cdot \mathbf{J}_C = +N \tag{11a}$$

$$\nabla \cdot \mathbf{J}_D = -N \tag{11b}$$

$\mathbf{J}_C$ and $\mathbf{J}_D$ represent the vectors of the molar flux density of NaCl in the concentrate and diluate solutions, respectively, N denotes a source/sink term, as discussed bellow. Convective and diffusive transport of NaCl is taken into account and the expression for $\mathbf{J}_C$ and $\mathbf{J}_D$ takes the form of Eq. (12).

$$\mathbf{J}_C = -\mathbf{D} \cdot \nabla c_C + \mathbf{v}_C c_C \tag{12a}$$

$$\mathbf{J}_D = -\mathbf{D} \cdot \nabla c_D + \mathbf{v}_D c_D \tag{12b}$$

Here $\mathbf{D}$ is an anisotropic diffusivity matrix with binary diffusivity components $D_{i,x}$ and $D_{i,y}$ in the direction of the x and y axes, respectively, see Expression (13). Subscript i indicates a model subdomain.

$$\mathbf{D} = \begin{pmatrix} D_{i,x} & 0 \\ 0 & D_{i,y} \end{pmatrix} \tag{13}$$

The values of the components of matrix $\mathbf{D}$ are summarized in Table 2. It should be noted that the components $D_{2,y}$, $D_{3,y}$ and $D_{4,y}$ are considered to be zero in the model because (i) the concentration gradients in the direction perpendicular to the membrane surface in subdomains 2, 3 and 4 are assumed to be negligible and (ii) the individual desalinating or concentrate compartments are mechanically separated by membranes in a real ED membrane stack. The diffusion coefficient of Na^+ or Cl^- in diluate water solution has a value of approx. $D_0 = 1 \times 10^{-9}\ \mathrm{m^2\ s^{-1}}$. Considering the typical mean velocity in the DC or CC of approx. $0.05\ \mathrm{m\ s^{-1}}$, this indicates that diffusive transport is significantly less important than convection. Therefore, to avoid convergence problems associated with a high Peclet number characterizing convective-diffusion mass transport, the values of diffusion coefficients used in this work were increased by several orders of magnitude (for the exact number, see Table 2) compared to D_0 instead of reducing the element size of the mesh discretization. The latter means of reducing the Peclet number would result in a significant increase in the computational demands of the model without a corresponding impact on its results. In subdomains 2, 3 and 4 the increase in diffusivity by three orders of magnitude was sufficient to provide a smooth convergence and at the same time low enough not to affect the local distribution of NaCl in the system significantly. In the subdomains of the feed and drain channels the diffusion coefficients are increased by 4 and 5 orders of magnitude because of the proportionally higher convective flow velocity in these subdomains. Moreover, the high diffusion coefficient in the direction of the x-coordinate fulfils the role of intensive convective mixing of the solution in this direction. This convective mixing is neglected in the present model because it takes simplified potential flow conditions into account. A description of the solution hydrodynamics is given later in the text. c_D and c_C in Eq. (12) represent local concentrations of NaCl in the diluate and concentrate solutions, respectively. $\mathbf{v}_D$ and $\mathbf{v}_C$ then denote the local velocity vectors of the diluate and concentrate solution flows, respectively.

The contribution of migration to the transport of solute along the x-axis is considered negligible compared to the convective transport. On the other hand, ion migration in the direction normal to the membrane surface is responsible for NaCl transfer from the DC to the CC described by

Table 2 Binary diffusion coefficients of NaCl in diffusion matrix $\mathbf{D}$ ($\mathrm{m^2\ s^{-1}}$)

Subdomain Direction	1	2	3	4	5
x-coordinate	$D_0 \times 10^5$	$D_0 \times 10^3$	$D_0 \times 10^3$	$D_0 \times 10^3$	$D_0 \times 10^5$
y-coordinate	$D_0 \times 10^4$	0	0	0	$D_0 \times 10^4$

the source/sink term N in the balance Eq. (11). N is expressed by Eq. (14) and plus and minus signs distinguish whether N represents a source or a sink, respectively.

$$N = \frac{\psi}{Fh_p} j_y + \mu(c_C - c_D) \tag{14}$$

The amount of solute transferred from the DC to the CC is proportional to the component of current density normal to the membrane surface j_y. The overall efficiency of solute transfer by migration is given by empirical parameter ψ. This parameter corrects discrepancies between the proposed mathematical model and reality, stemming mainly from (i) omission of electro-osmosis and (ii) non-ideal selectivity of real membranes in the model. At lower current loads corresponding to a medium degree of desalination, the overall efficiency ψ can be supposed to be constant. At even lower degree of desalination, below approximately 30 %, the value of ψ is close to 1, which is the case in the present study. The solute transport between the CC and DC not directly related to the electric current is described by the second term on the right-hand side of Eq. (14). This flux is proportional to the concentration difference of the solute in the individual compartments and to the overall solute permeability μ. Since one of the main non-faradaic solute transfer mechanisms is backward diffusion from the CC to the DC due to the large difference in solute concentration, the solute permeability is negative and has a value of around -1×10^{-4} s^{-1}.

3.3 Convective flow of the process solutions

The convective flow of the process solutions is governed by a continuity equation represented by Eq. (15) corresponding to the diluate and concentrate streams.

$$\nabla \cdot \mathbf{v}_C = +Q = 0 \tag{15a}$$

$$\nabla \cdot \mathbf{v}_D = -Q = 0 \tag{15b}$$

As stated above, the crossover of the solvent through the membranes is relatively small compared to the volumetric flow rate through one compartment, therefore it is neglected in the continuity equations, i.e. source/sink term Q is considered equal to zero. However, a general description of this phenomenon includes two effects, electro-osmosis and osmosis, where the former is proportional to the current density normal to the membrane surface and electro-osmotic coefficient β, while the latter is driven by the concentration difference across the membrane and proportional to the solvent permeation coefficient π, according to Eq. (16).

$$Q = \beta j_y + \pi(c_C - c_D) \tag{16}$$

The local convective velocities $\mathbf{v}_D$ and $\mathbf{v}_C$ of the diluate and concentrate solutions, respectively, are identically described by means of an anisotropic Darcy's law, i.e. the velocity is proportional to the pressure gradient according to Eq. (17).

$$\mathbf{v}_C = -\mathbf{P}_C \cdot \nabla p_C \tag{17a}$$

$$\mathbf{v}_D = -\mathbf{P}_D \cdot \nabla p_D \tag{17b}$$

The hydraulic permeability of the system for the solution flow is given by the permeability tensors $\mathbf{P}_C$ and $\mathbf{P}_D$ defined by Expression (18).

$$\mathbf{P}_C = \mathbf{P}_D = \mathbf{P} = \begin{pmatrix} \kappa_H P_{i,x} & 0 \\ 0 & \kappa_H P_{i,y} \end{pmatrix} \tag{18}$$

Permeability tensors for the diluate and concentrate streams are equal because of the symmetrical geometry of the net-like spacer in the DC and CC. The components of tensor $\mathbf{P}$ take different values in the individual subdomains i because of the variable free cross-sectional flow area. The difference between $P_{i,x}$ and $P_{i,y}$ is then given by the system anisotropy resulting from the fact that the membranes are considered to be impermeable to liquid and thus the solution flow is preferred in a certain direction. The values of $P_{i,x}$ and $P_{i,y}$ are expressed by Eq. (19).

$$\begin{aligned}
&P_{1,x} = P_{5,x} = \kappa_B B f_{1,C} = \kappa_B B f_{1,D} \quad (\kappa_B = 300)\\
&P_{2,x} = \kappa_B B f_{2,D} = \kappa_B B f_{2,C} \quad (\kappa_B = 0.5)\\
&P_{3,x} = \kappa_B B f_{3,D} = \kappa_B B f_{3,C} \quad (\kappa_B = 2/3)\\
&P_{4,x} = \kappa_B B f_{4,D} = \kappa_B B f_{4,C} \quad (\kappa_B = 0.25)\\
&P_{2,y} = P_{3,y} = P_{4,y} = 0\\
&P_{1,y} = P_{5,y} = \kappa_B B f_{1,C} = \kappa_B B f_{1,D} \quad (\kappa_B = 2)\\
&B = \frac{h_D^2}{12\eta} = \frac{h_C^2}{12\eta}
\end{aligned} \tag{19}$$

The permeability of the system is calculated from the product of isotropic Darcy's coefficient B, volumetric fraction of the space filled by solution $f_{i,j}$ and a correction coefficient κ_B. $f_{i,j}$ defined by Expression (9) represents a correction for the presence of the spacer-net in the working chambers and for the deviations between the real 3D system and the simplified 2D macrohomogeneous model geometry in the individual model subdomains. Parameter B is derived analytically for a 2D narrow rectangular channel in-between two parallel plates and under laminar flow conditions. For more details, see the literature [16–18]. B mainly includes the effect of friction forces between the channel walls and the liquid. Based on the similarity principle, coefficient B is used to evaluate the permeability in the working chambers free of spacer net and under the assumption of ideally flat membranes. However, the spacer net introduces an additional solid–liquid contact area into the channel and also disturbs the ideally laminar flow character. These effects result in lower permeability of the working chamber. Therefore $\kappa_B = 2/3$

is used to correct the value of B in the expression for $P_{3,x}$ to obtain closer agreement with reality. Similar corrections $\kappa_B = 0.5$ and $\kappa_B = 0.25$ were used in the case of $P_{2,x}$, and $P_{4,x}$, respectively, i.e. the apparent permeability of the distribution channels is lower than B because of the transient or turbulent flow regime in these domains. The above values of κ_B, corresponding to $P_{2,x}$, $P_{3,x}$ and $P_{4,x}$, were estimated from the experimental measurements of the pressure field in the intermembrane space presented in paper [18]. To calculate the permeability in the subdomains of the feed and drain channels, parameter B is used rather as a reference value. $P_{1,x}$ and $P_{5,x}$ are significantly increased with respect to B to reduce the pressure gradient in these subdomains in the direction of the x-axis to a negligibly low value. In these cases a value of $\kappa_B = 300$ was considered sufficient. Higher permeability results from the fact that there are no upper and bottom walls in these subdomains to cause pressure dissipation in the x direction as there are in the narrow flat channel. In the case of $P_{1,y}$ and $P_{5,y}$, $\kappa_B = 2$. This is due to the around 10 times higher hydraulic diameter and 50 times higher mean Re number in the feed and drain channels, compared to the working chamber. While the increase in hydraulic diameter results in a permeability increase, the increase in Re number followed by the transition of the flow regime from viscous to turbulent leads to a formal decrease in channel permeability. It is worth noting that, at this stage, the corrections used to calculate the permeability of the individual subdomains have to be regarded as an approximation; a correct analysis of the flow hydrodynamics in the real apparatus is still required. This is further emphasized by the fact that hydraulic resistance of the reported ED unit model achieves approximately 15 % of that obtained experimentally for a real industrial ED unit. To compensate for this, an additional correction factor for hydraulic resistance κ_H was introduced into Expression (18). Its value of $\kappa_H = 1/7$ was set on the basis of the experimental data. An exact description of the flow hydrodynamics in the ED unit is, however, not the main aim of this paper, thus it will not be discussed here in more detail. Finally, permeabilities $P_{2,y}$, $P_{3,y}$ and $P_{4,y}$ are set equal to zero because membranes are considered impermeable to liquid.

3.4 Boundary conditions

In this model, Dirichlet and Neumann boundary conditions, summarized in Table 3, are used. The numbering of the individual boundaries is indicated in Fig. 3. Some of the boundary conditions call for a more detailed explanation. The cathode (boundary no. 9) is represented by an 1D electrode–electrolyte interface characterized by constant Galvani potential at a zero reference level. By contrast, the anode is represented by a 2D subdomain. The only migration transfer of charge is considered inside the anode body governed by a charge balance, see Eq. (1). The current density in the anode body is calculated from $j = \sigma_A \nabla \phi$, where σ_A is the specific conductivity of the anode material. σ_A is considered constant and is intentionally increased in the model. The incorporation into the model geometry of an anode body with high electric conductivity allowed the application of constant current density $j_{in} = I/(d \times l_3)$ (I corresponds to the current load) to the current feeder boundary (no. 11), while simultaneously keeping a constant Galvani potential along the electrode–electrolyte interface (no. 10). This means that the potential difference between the electrodes at the entrance to the working chambers is regarded as almost the same as the value at the exit region. Infinitely fast electrode reaction kinetics is considered because of its negligible effect on the total voltage and behaviour of the ED unit.

The solution inlet (no. 3) is characterized by constant inlet velocity v_{in}, determined from the total volumetric flow rate. A zero reference pressure is applied at the solution outlet (no. 17), thus the pressure calculated at the inlet corresponds to the total pressure drop in the ED unit (Δp). The inlet boundary (no. 3) is also characterized by molar concentration at the inlet of NaCl c_{in}. The solute only leaves the system through the outlet boundary (no. 17) via convection. NaCl diffusion does not occur across this boundary.

The transport of solute and solution convective flow are not considered by the model in the anode subdomain, thus

Table 3 Boundary conditions

Boundary no.	Description	Boundary conditions				
11	Anode feeder	$-\mathbf{n} \cdot \sigma_A \nabla \phi = j_{in}$	–	–	–	–
9	Cathode	$\phi = 0$	$\mathbf{n} \cdot \nabla c_C = 0$	$\mathbf{n} \cdot \nabla c_D = 0$	$\mathbf{n} \cdot \nabla p_C = 0$	$\mathbf{n} \cdot \nabla p_D = 0$
3	Solution inlet	$\mathbf{n} \cdot \nabla \phi = 0$	$c_C = c_{in}$	$c_D = c_{in}$	$-\mathbf{n} \cdot \nabla p_C = v_{in}$	$-\mathbf{n} \cdot \nabla p_D = v_{in}$
17	Solution outlet	$\mathbf{n} \cdot \nabla \phi = 0$	$\mathbf{n} \cdot \nabla c_C = 0$	$\mathbf{n} \cdot \nabla c_D = 0$	$p_C = 0$	$p_D = 0$
8, 13	Walls	$\mathbf{n} \cdot \nabla \phi = 0$	–	–	–	–
1, 2, 5, 6, 14, 15, 18, 19	Walls	$\mathbf{n} \cdot \nabla \phi = 0$	$\mathbf{n} \cdot \nabla c_C = 0$	$\mathbf{n} \cdot \nabla c_D = 0$	$\mathbf{n} \cdot \nabla p_C = 0$	$\mathbf{n} \cdot \nabla p_D = 0$
4, 7, 10, 12, 16	Internal boundaries			Continuity		

the corresponding boundary conditions are not specified at the anode boundaries (nos. 8, 11 and 13).

3.5 Model summary and numerical solution

The proposed model consists of five dependent variables: Galvani potential ϕ described by Eq. (1), molar concentration of NaCl in the diluate and concentrate solutions c_D and c_C, respectively, determined by Eq. (11) and pressure in the diluate and concentrate solutions p_D and p_C, respectively, calculated by means of Eq. (15). The set of model PDEs was solved by the finite element method implemented in the COMSOL Multiphysics™ environment. The model was first solved for trivial solution at zero current density j_{in}. Subsequently, j_{in} was continuously increased, while the previous solution was used as an initial guess for the subsequent parameter step. This procedure allowed a smooth convergence of the model.

4 Experimental part

Experimental data used for validation of the mathematical model were obtained for a water desalination process performed using a commercial, industrial-scale ED unit EDR-III/500/0.8 supplied by MEGA a.s. [30]. The experimental ED unit consists of 500 membrane pairs. RALEX AMH-PES and RALEX CMH-PES are used as the AM and CM, respectively. The membranes are separated by flow-sheet net-like spacers similar to those shown in Fig. 2A, B. The total active area of one membrane is equal to 0.42 m^2 with dimensions of the working chamber of 0.32 × 1.30 m^2. The remaining parameters of the experimental system are summarized in Tables 1 and 4. As already given, EDR-III/500/0.8 represents a commercial unit and detail information on its internal geometry and operational parameters cannot be disclosed at this place. Therefore after validation of the model using experimental data from this unit in Sect. 5.1 following parametric studies were performed using the geometry corresponding to the virtual unit. The later one has a different configuration in terms of the number of membrane pairs and the length of the working chamber. The reduced dimensions enabled a corresponding reduction of the hardware and time demands of the model. Since the process streams flow hydrodynamics is calculated in parallel to the local mass and charge flow distribution, reduction of number of the membrane pairs has no impact on the model results accuracy.

The experimental measurements were performed in a batch configuration with recirculation of the process solution. A solution reservoir with a volume of 2 m^3 was used. An identical solution was circulated through the DCs and CCs with an equal, constant volumetric flow rate in the range of 25–35 $m^3\ h^{-1}$ (flow meter GEORG FISHER +GF+). This corresponds to mean linear velocities in the working chamber at an interval of $\bar{v} = 5.43 \times 10^{-2}$–$7.6 \times 10^{-2}$ m s^{-1}. The diluate and concentrate solutions drained out of the ED unit were again mixed in the solution reservoir, thus the salt concentration in the reservoir did not change in time. This allowed stationary measurements of the ED unit performance. The process solution used was a water solution of NaCl with a molar concentration in the range of 1.40×10^{-2}–9.86×10^{-2} mol dm^{-3}. The measurements were performed at a temperature of 22 ± 5 °C. The electrodes were washed by Na_2SO_4 solution with a volumetric flow rate of 0.5 $m^3\ h^{-1}$.

The ED unit was operated at a constant voltage in the range of 0–300 V (DC source NAPAZ ± 350 V), while the current load was recorded. The NaCl outlet concentration was determined using the specific conductivity (laboratory multimeter pH/Cond 340i WTW) of the outlet solution. The value of the concentration was obtained by interpolating the table data [29] valid for the temperature of the outlet solution.

5 Results and discussions

5.1 Experimental validation of the model results

The experimentally observed voltage drop on the SMP together with the obtained global degree of desalination (GDD) defined by Eq. (20) are plotted in dependence on the applied current density j_{in} for three different experimental conditions in Fig. 4. The mathematical model results are shown in the same figure for comparison. A comparison of the model and experimental data is provided for a medium degree (up to 55 %) of GDD for which the model was designed.

$$\mathrm{GDD} = \left(1 - \frac{c_{D(17)}}{c_{D(3)}}\right) 100\% \tag{20}$$

The three different operational conditions studied resulted in different degrees of desalination. First, the values of U_p were compared. The results of the basic mathematical model exhibited values corresponding approximately to 50 % of the experimental ones, see the solid line 1 in figures subset 1. The main reason for this discrepancy is the electrical resistance of the ED stack which was underestimated in the model, resulting to a large extent from: (a) a shortening of the ionic current pathways due to the simplification of the geometry from 3D to 2D, (b) the discrepancy between the used and the actual value of specific conductivity of the membrane, (c) an underestimation of the electrical resistance of the diluate solution in the diluate compartment due to neglecting the existence

Table 4 Input parameters

Symbol	Value	Unit	Description
R	8.314	J K^{-1} mol^{-1}	Universal gas constant
T	298.15	K	Temperature
F	96,485	C mol^{-1}	Faraday constant
D_0	1×10^{-9}	m^2 s^{-1}	Diffusion coefficient of Na^+ or Cl^- in water solution
ψ	1		Overall current efficiency
μ	-1×10^{-4}	s^{-1}	Overall NaCl permeability across membranes
η	0.8908×10^{-3}	Pa s	Dynamic viscosity of water
σ_A	1×10^4	S m^{-1}	Specific conductivity of anode body
σ_{AM}	0.8158	S m^{-1}	Specific conductivity of AM (RALEX AMH-PES [30])
σ_{CM}	0.9781	S m^{-1}	Specific conductivity of CM (RALEX CMH-PES [30])
c_{in}	0.2567	mol dm^{-3}	Inlet concentration of NaCl in the diluate and concentrate solutions (it corresponds to 15 g dm^{-3} of NaCl, which is typical of brackish waters)
κ_R	0.57		Dimensionless empirical parameter correcting the electrical resistance of the ED membrane stack
Q	8	m^3 h^{-1}	Volumetric flow rate through the studied ED unit
$\bar{v}_{real}$	0.0434	m s^{-1}	Real mean convective velocity of the solution in the working compartments
$\bar{v}_D = \bar{v}_C$	0.0127	m s^{-1}	Mean calculated convective velocity of the solution in the working compartments
v_{in}	0.0798	m s^{-1}	Inlet velocity of the diluate or concentrate solution applied at boundary no. 3
Δp	40	kPa	Total pressure drop in the studied ED unit

of the Nernst diffusion layer, (d) an underestimation of the membrane potential. It can, however, be assumed that with low degrees of desalination all of these effects contribute linearly to the electrical resistance of the ED stack. Only effects (c) and (d) can be considered negligible at a low GDD and current load range. To eliminate all the above-mentioned effects an empirical constant κ_R, increasing the ohmic resistance of the ED stack in the direction of the y-coordinate, was introduced into the model, see Eq. (4). κ_R was evaluated by means of the experimental data for low GDD $\leq$ 25 % corresponding to case (C), see Fig. 4C1, C2. For $\kappa_R = 0.57$ an excellent agreement was obtained between U_p determined experimentally and calculated by the model. As can be seen in Fig. 4A1, B1, the agreement is also found under different operational conditions, though limited to GDD $\leq$ 25 %. At a higher GDD the dependence of U_p on j becomes nonlinear and U_p obtained experimentally increases more progressively than that calculated by the mathematical model. This is because at higher GDD the importance of U_M and the non-ideal behaviour of the membranes significantly increase with increasing current density. This trend is probably connected with an increase in the electrical resistance of the diluate solution due to the formation of an Nernst diffusion layer not considered in the model. These results, therefore, demonstrate the application limits of the presented version of the mathematical model. However, these application limits are imposed by the simplification of the ED process physics introduced here rather than by the adoption of an assumption about the system's macrohomogeneity.

With respect to the GDD as the second parameter investigated, it was observed both experimentally and by means of the mathematical model that it increased linearly with j throughout the range of conditions under study, see figures subset 2 in Fig. 4. For comparison, theoretical maximum values of the GDD calculated from the model of zero dimension (0D), i.e. material balance for ideal electric current efficiency ($\psi = 1$) and ideal membrane selectivity ($\mu = 0$), are also shown. As can be seen, the results of the mathematical model exhibit slightly lower values compared to the maximum theoretical ones. This was caused by the existence of parasitic current passing through the feed and drain channels outside the working chambers of the membrane stack not considered by the 0D material balance. In the case of the ED process, the value of parasitic current depends mainly on the ratio of the electrical resistance of the central working part of the membrane stack to the electrical resistance of the surrounding hydraulic circuitry (i.e. feed and drain channels and inlet distribution and outlet collecting channels). This ratio is generally low.

A very low value of parasitic current was observed experimentally under the operational conditions corresponding to case C, see Fig. 4C2, where the experimental data are in agreement with the theoretical 0D material balance. However, the experimentally determined values of the GDD, corresponding to cases A and B, see Fig. 4A2, B2, exhibit higher values than the theoretical ones. These experimental data thus exceed the material balance of the system, which indicates experimental error. Therefore,

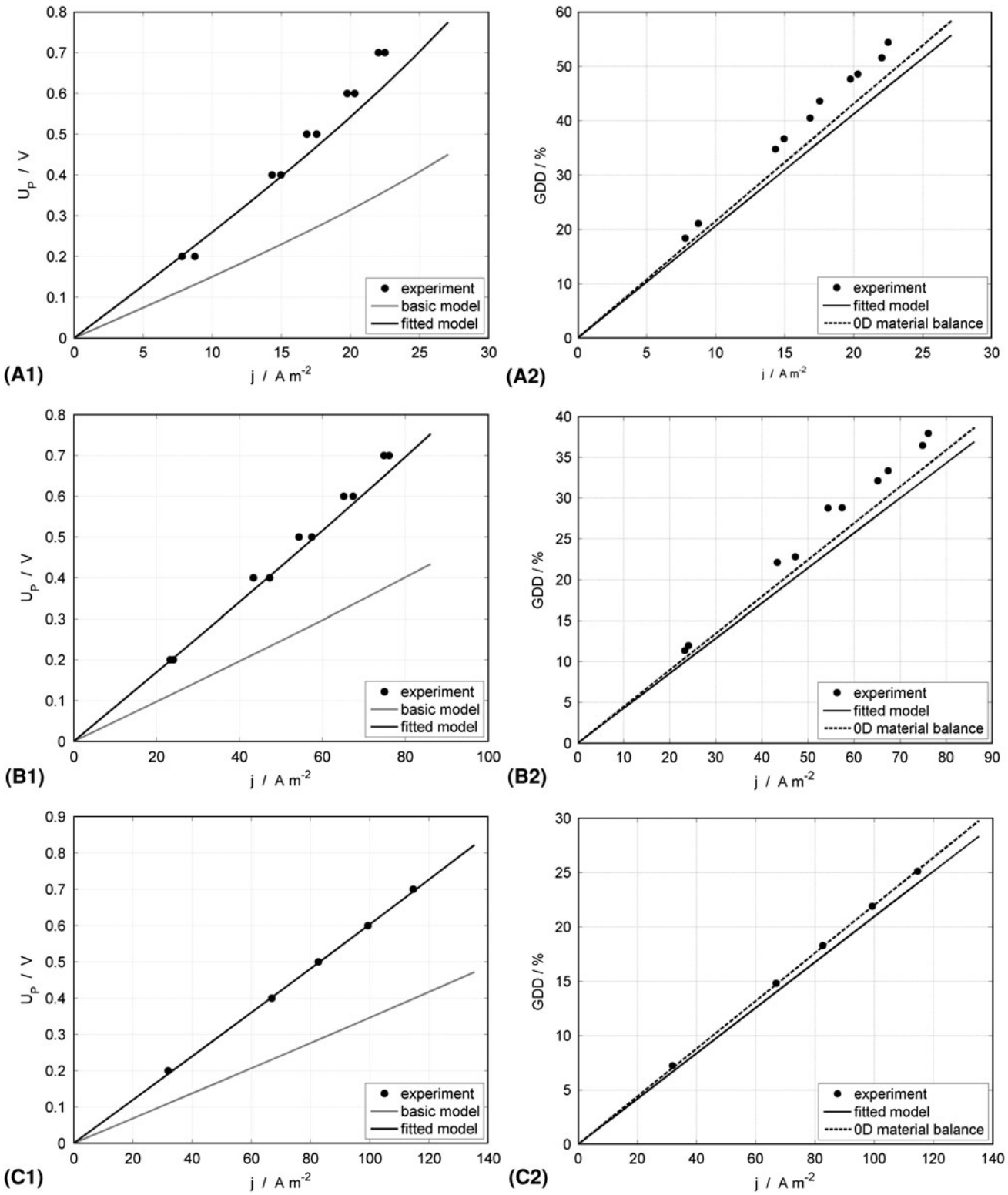

Fig. 4 Voltage drop on one membrane pair (series 1) and global degree of desalination (series 2) in dependence on applied current density under different operational conditions: **A** $\bar{v}_{\text{real}} = 5.43 \times 10^{-2}$ m s^{-1}, $c_{\text{in}} = 1.40 \times 10^{-2}$ mol dm^{-3}, **B** $\bar{v}_{\text{real}} = 6.51 \times 10^{-2}$ m s^{-1}, $c_{\text{in}} = 5.64 \times 10^{-2}$ mol dm^{-3}, **C** $\bar{v}_{\text{real}} = 7.6 \times 10^{-2}$ m s^{-1}, $c_{\text{in}} = 9.86 \times 10^{-2}$ mol dm^{-3}; *points* experimental data; *solid lines* mathematical model results, *grey solid line* basic model (in figures of series 1), *black solid line* model results with fitted empirical constant $\kappa_{\text{R}} = 0.57$; *black dashed line* (upper line in figure) maximum theoretical GDD based on mass balance for $\psi = 1$ and $\mu = 0$ s^{-1}

these experimental data do not allow an evaluation of the parasitic current. In other words, the value of parasitic current is below the detection limit of the experimental set-up, therefore it is not possible for the experimental data to validate the parasitic current calculated by the model.

5.2 Local distribution of the basic model quantities

The main advantage of the macrohomogeneous model concept presented consists in the possibility to evaluate the local distribution of the important quantities inside the ED stack. The local distribution of these quantities determined by the presented mathematical model fitted for $\kappa_R = 0.57$, the uniform flow hydrodynamics and operational condition of the brackish water desalination will be discussed in this section. The input parameters used are summarized in Table 4. Concurrent solution flow in DCs and CCs is considered. The uniformity of the distribution of the diluate or concentrate solution into the respective compartments is apparent from the streamlines shown in Fig. 5. Due to energy dissipation, a moderate pressure gradient may be observed in the feed and drain channels. It results in a moderate variation of the pressure difference between the feed and drain channels along the y-coordinate. This difference is lowest in the middle of the ED stack and it leads to minimum linear velocity v_D or v_C in the central working chamber, see Fig. 9a (line 4). After exceeding this point, the pressure difference and correspondingly v_D and v_C increase. Note that the calculated linear velocities v_D or v_C in the working chambers are lower than the linear velocity in the real ED unit v_{real} so, as $v_{real} = \frac{v_D}{f_{3,D}} = \frac{v_C}{f_{3,C}}$. The explanation is that the cross-sectional area of the DCs or CCs in the real ED unit is lower in comparison to the flow cross-sectional area of the subdomain of the working chambers in the model geometry (given by $h_1 \times d$). Accordingly to the cross-section area change, the mean linear velocity over all diluate or concentrate compartments $\bar{v}_{real}$ is higher than the mean linear velocities calculated by the model $\bar{v}_D = \bar{v}_C = \frac{Q}{h_1 \cdot d}$, i.e. $\bar{v}_{real} = \frac{\bar{v}_D}{f_{3,D}} = \frac{\bar{v}_C}{f_{3,C}}$. Owing to the uniform flow hydrodynamics, the desalination of the diluate solution takes place almost uniformly in the entire membrane stack as well, as can be seen in Fig. 6A1, A2, both at medium (GDD = 39 %) and high (GDD = 79 %) current loads. The desalination in the central diluate compartment takes place to a slightly higher degree on account of the slightly lower linear velocity in this compartment, as discussed above.

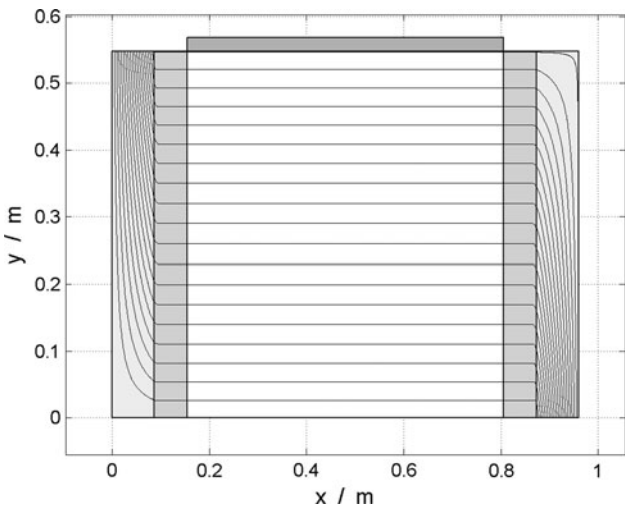

Fig. 5 Streamlines of the solution flow through the ED unit—identical for diluate and concentrate solution flow; parameters for diluate or concentrate stream: $Q = 8\ m^3\ h^{-1}$, $\bar{v}_{real} = 0.043\ m\ s^{-1}$, $\Delta p = 40$ kPa

The distribution of Galvani potential for the same model situation is presented in Fig. 6B1, B2. The values of Galvani potential in this figure are normalised to the cell voltage. In these figures there is no apparent difference between the distribution of the Galvani potential at the two levels of current load studied. Moreover, in both cases the potential field is almost ideally symmetrical with respect to the centre of the membrane stack, which indicates an ideal situation with homogeneous distribution of the local current density values inside the ED stack. This mainly corresponds to (a) the negligible impact of the membrane potential calculated by Eq. (3) and (b) the minor changes in the overall specific conductivity of the membrane stack, the latter aspect being caused by compensation for the decrease in the specific conductivity of the diluate along the channel by the conductivity increase in the concentrate solution. The Galvani potential gradient in the feed and drain channels indicates the existence of parasitic current.

The electric current lines corresponding to the Galvani potential gradients inside the ED unit are shown in Fig. 6C1, C2. As follows from the homogeneous and symmetrical distribution of the Galvani potential isolines, the course of the current lines in the working part of the membrane stack is almost parallel. Current lines passing through subdomains 1, 2, 4 and 5 correspond to the parasitic current. Since parasitic current flows outside the working part of the membrane stack, it does not contribute to the desalination of the diluate solution, which thus represents energy losses of the entire process. Compared to the Galvani potential fields, changes in the current line distribution are more pronounced with increasing current load.

The uniformity of the local current density distribution in the working part of the membrane stack can be assessed from Fig. 7. In this figure, local values of the y-component of current density (normal to the membrane surface) divided by current density averaged over the working surface area of the membrane are shown in dependence on the

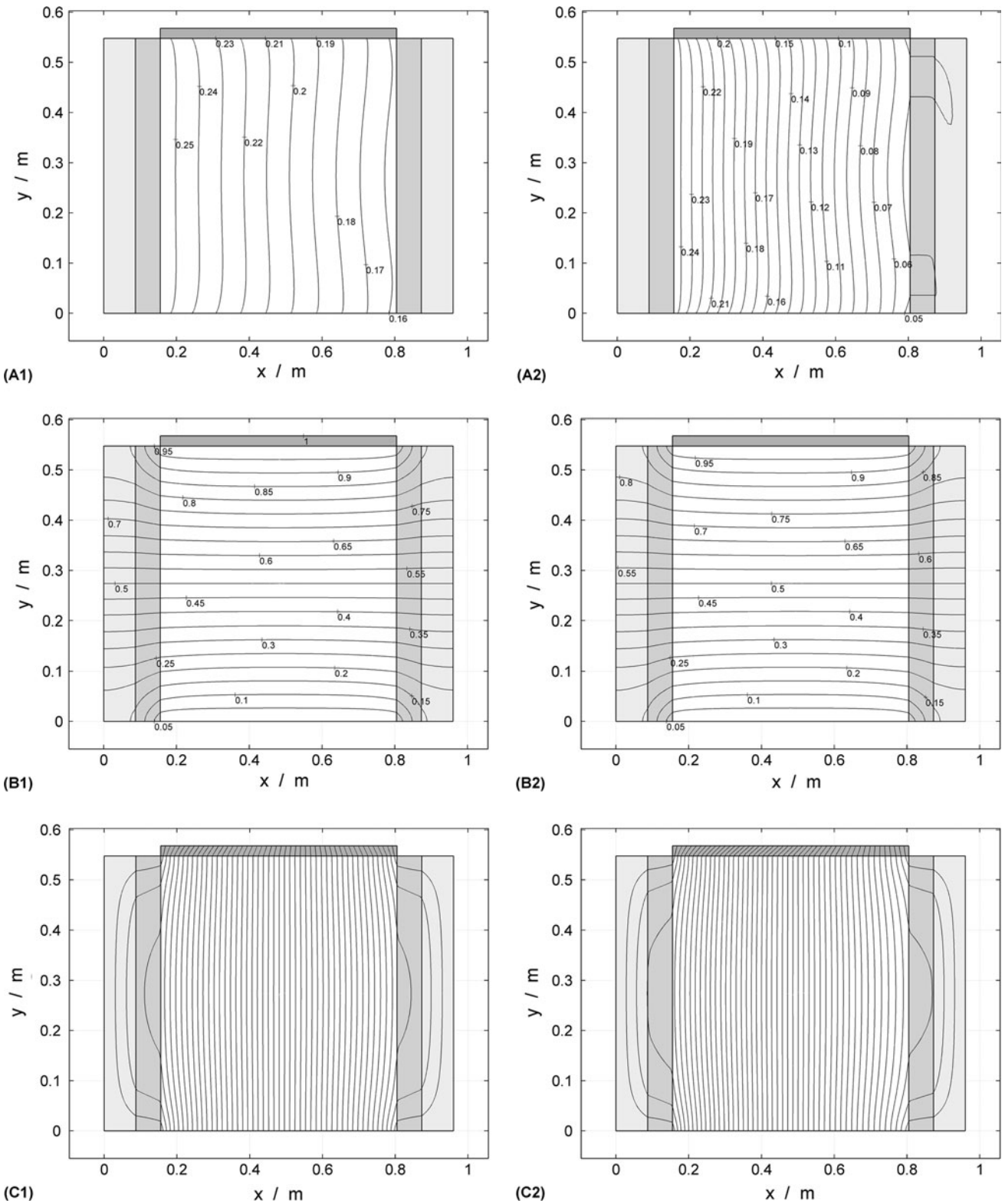

Fig. 6 **A** Isolines of the local NaCl concentration in the diluate stream in (mol dm^{-3}). **B** Isolines of the local Galvani potential normalised to the total voltage of the ED unit. **C** Electric current lines in the ED unit; (series 1) medium current load $I = 120$ A ($j = 577$ A m^{-2}, GDD = 39 %, $U = 376.5$ V, $U_p = 1.9$ V); (series 2) high current load $I = 240$ A ($j = 1154$ A m^{-2}, GDD = 77 %, $U = 815$ V, $U_p = 4.1$ V); other operational parameters: $Q = 8$ m^3 h^{-1}, $\bar{v}_{real} = 0.043$ m s^{-1}, $\Delta p = 40$ kPa, $c_{in} = 0.257$ mol dm^{-3}

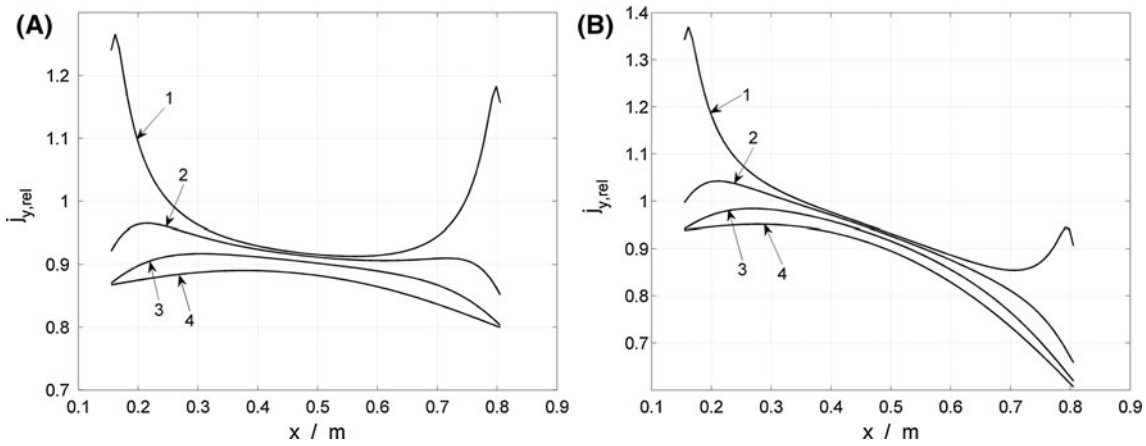

Fig. 7 Dependence of current density normal to the membrane surface on the position along the x-axis at various positions y on the membrane stack; values of current density are normalised to the average current density at the anode surface j_{in}; **A** current load $I = 120$ A ($j_{in} = 577$ A m^{-2}, GDD = 39 %, $U = 376.5$ V, $U_p = 1.9$ V); **B** current load $I = 240$ A ($j_{in} = 1154$ A m^{-2}, GDD = 77 %, $U = 815$ V, $U_p = 4.1$ V); positions along the membrane stack: (*1*) $y = 0 \times h_1$ cm (cathode surface), (*2*) $y = 0.1 \times h_1$ cm, (*3*) $y = 0.2 \times h_1$ cm, (*4*) $y = 0.5 \times h_1$ cm (centre of the membrane stack), the distribution of current density is symmetrical along the central axis at $y = 0.5 \times h_1$ cm; remaining operational parameters: $Q = 8$ m^3 h^{-1}, $\bar{v}_{real} = 0.043$ m s^{-1}, $\Delta p = 40$ kPa, $c_{in} = 0.257$ mol dm^{-3}

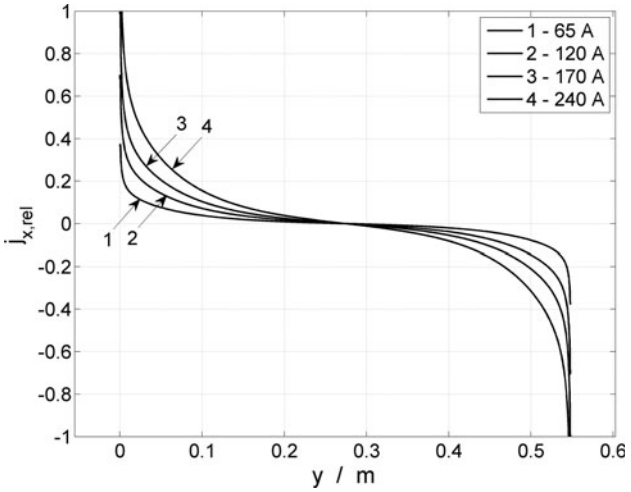

Fig. 8 Dependence of value of x-component of current density vector along the boundary 7 (interface between inlet distribution channels and working chambers) on the position along the ED stack; values of j_x normalised to the average value at the anode feeder j_{in}; four different current loads: (*1*) $I = 65$ A ($j_{in} = 312.5$ A m^{-2}, GDD = 21 %, $U = 201.5$ V, $U_p = 1$ V), (*2*) $I = 120$ A ($j_{in} = 577$ A m^{-2}, GDD = 39 %, $U = 376.5$ V, $U_p = 1.9$ V), (*3*) $I = 170$ A ($j_{in} = 817$ A m^{-2}, GDD = 55 %, $U = 544.5$ V, $U_p = 2.7$ V), (*4*) $I = 240$ A ($j_{in} = 1154$ A m^{-2}, GDD = 77 %, $U = 815$ V, $U_p = 4.1$ V); remaining operational parameters: $Q = 8$ m^3 h^{-1}, $\bar{v}_{real} = 0.043$ m s^{-1}, $\Delta p = 40$ kPa, $c_{in} = 0.257$ mol dm^{-3}

position along the channel. Since the electrode has the same working surface area as the membrane, the average value of the current density is equal to j_{in} applied at the current feeder boundary (no. 11). It is important to consider that only the y-component of current density is responsible for NaCl transfer from the diluate to the concentrate stream. The distribution of $j_{y,rel}$ is symmetrical with respect to the axis going through the centre of the membrane stack at $y = 0.5 \times h_1$, i.e. the distribution of $j_{y,rel}$ at the cathode is similar to that along the anode, etc. On the other hand, there is asymmetry in the distribution of $j_{y,rel}$ between the inlet and outlet regions. This is caused by a decrease in the diluate solution concentration resulting in an increase in membrane potential and a decrease in overall specific conductivity, as discussed above. Clearly, this effect is more pronounced in the case of high current loads leading to a higher degree of desalination, see Fig. 7B, compared to medium current loads, see Fig. 7A. Moreover, $j_{y,rel}$ decreases from the electrode towards the membrane stack centre because the value of the parasitic current flowing through the feed and drain channels increases in this direction. Another consequence of the parasitic current is that at the electrode surface $j_{y,rel}$ increases from the centre towards the electrode edges. This effect is well known as the edge (or corner) effect. However, near the electrode edges $j_{y,rel}$ passes over a maximum and then decreases up to the electrode edges due to the changing orientation of the current. Near the edge, the importance of the current component oriented in the direction x, i.e. parallel to the membrane surface, increases. Its y component thus decreases. This effect is apparent in the membrane stack in the vicinity of the electrode, see curve 2 in Fig. 7A. The maximum value of $j_{y,rel}$ decreases with increasing distance from the electrode due to the effect discussed above (parasitic current increase). Closer to the stack centre, the effect of parasitic current causes the appearance of just one maximum of the current density positioned slightly asymmetrically in the centre of the channel.

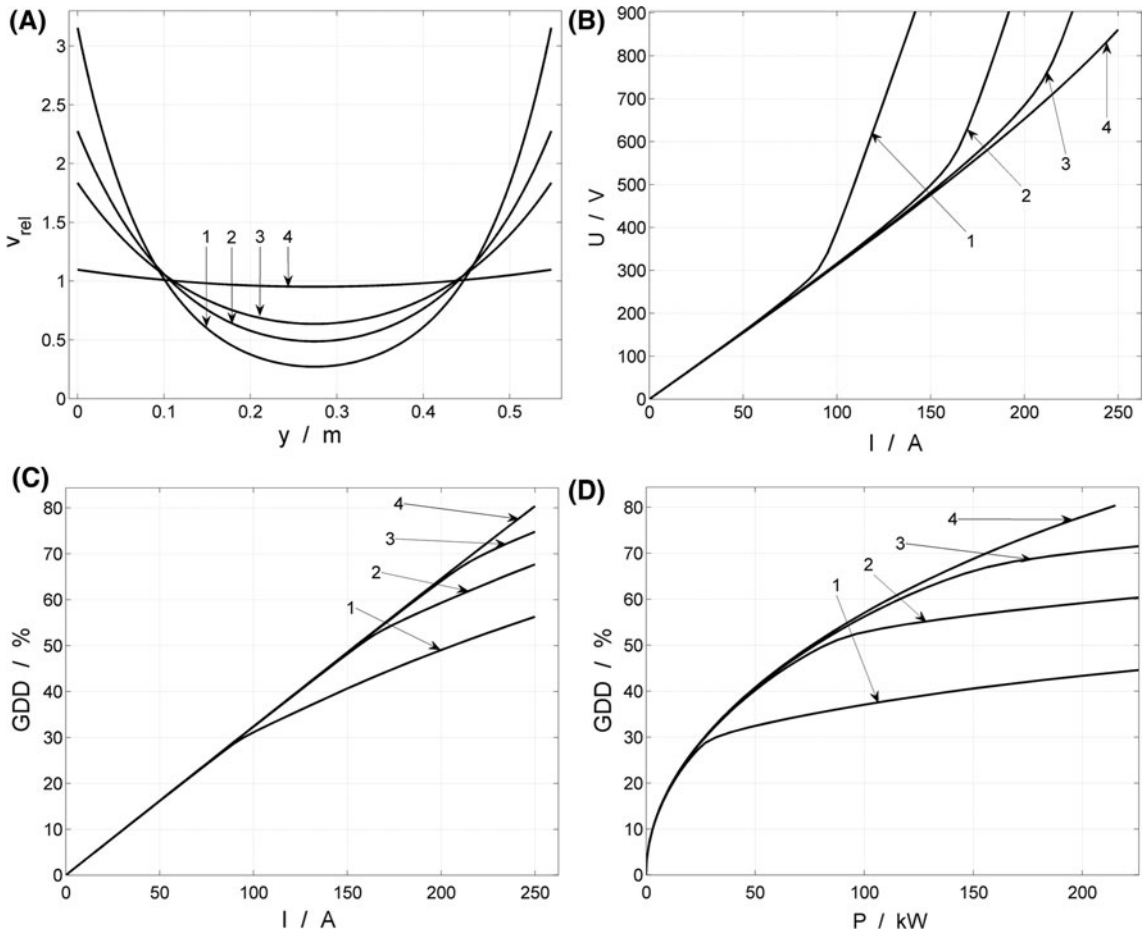

Fig. 9 **A** Variation of linear velocity in the working chambers along the membrane stack (along the *y*-axis), values of the linear velocity normalised to the average value, i.e. $v_{\text{real}} = \frac{v_{\text{D}}}{\bar{v}_{\text{D}}} = \frac{v_{\text{C}}}{\bar{v}_{\text{C}}}$. **B** Dependence of the stack voltage on the applied current. **C** Dependence of global degree of desalination on the stack current load. **D** Dependence of global degree of desalination on electric power input; variable uniformity of flow hydrodynamics: values of κ_{15y}: (*1*) $\kappa_{15y} = 0.03$ (extremely non-uniform), (*2*) $\kappa_{15y} = 0.06$, (*3*) $\kappa_{15y} = 0.1$, (*4*) $\kappa_{15y} = 1$ (uniform); remaining operational parameters: $Q = 8\ \text{m}^3\ \text{h}^{-1}$, $\bar{v}_{\text{real}} = 0.043\ \text{m s}^{-1}$, $\bar{v}_{\text{C}} = \bar{v}_{\text{D}} = 0.0127\ \text{m s}^{-1}$, $\Delta p = 40$ up to 375 kPa, $c_{\text{in}} = 0.257\ \text{mol dm}^{-3}$

This situation is further documented by Fig. 8. It shows the dependence of the *x*-component of the current density at the interface between the working part of the membrane stack and the domain of the inlet distribution channels on the position along the ED stack. In this case the current density is also divided by j_{in} to obtain a dimensionless value, permitting a comparison of the behaviour of the system under different current loads. The sign of $j_{x,\text{rel}}$ is negative in the part of the membrane stack closer to the anode. Here the current leaves the working chambers and becomes parasitic current. On the other hand, $j_{x,\text{rel}}$ is positive at the cathode part of the membrane stack, indicating a change in its flow direction, i.e. parasitic current flows back to the working chambers. In accordance with the previous observations, the value of $j_{x,\text{rel}}$ is highest in the vicinity of the electrodes and decreases towards the stack centre. Moreover, the relative value of j_x grows with increasing current load, which emphasizes the increase in the relative portion of parasitic current with increasing current load. This observation is in accordance with the growth in the electrical resistance of the working part of the membrane stack as the current load increases. The distribution of $j_{x,\text{rel}}$ along the interface of the outlet collecting channel is qualitatively similar to that at the inlet distribution channels, but the values are lower. This indicates that the parasitic current passing through the drain channels is slightly lower compared to the parasitic current in the feed channels, which is due to the lower specific conductivity of the domain of the drain channels.

5.3 Impact of irregularities of flow hydrodynamics

As it is known and as was substantiated by previous results, the homogeneity of the flow hydrodynamics inside the ED stack represents a crucial aspect with a detrimental impact on the stack's behaviour. Therefore, attention focussed on

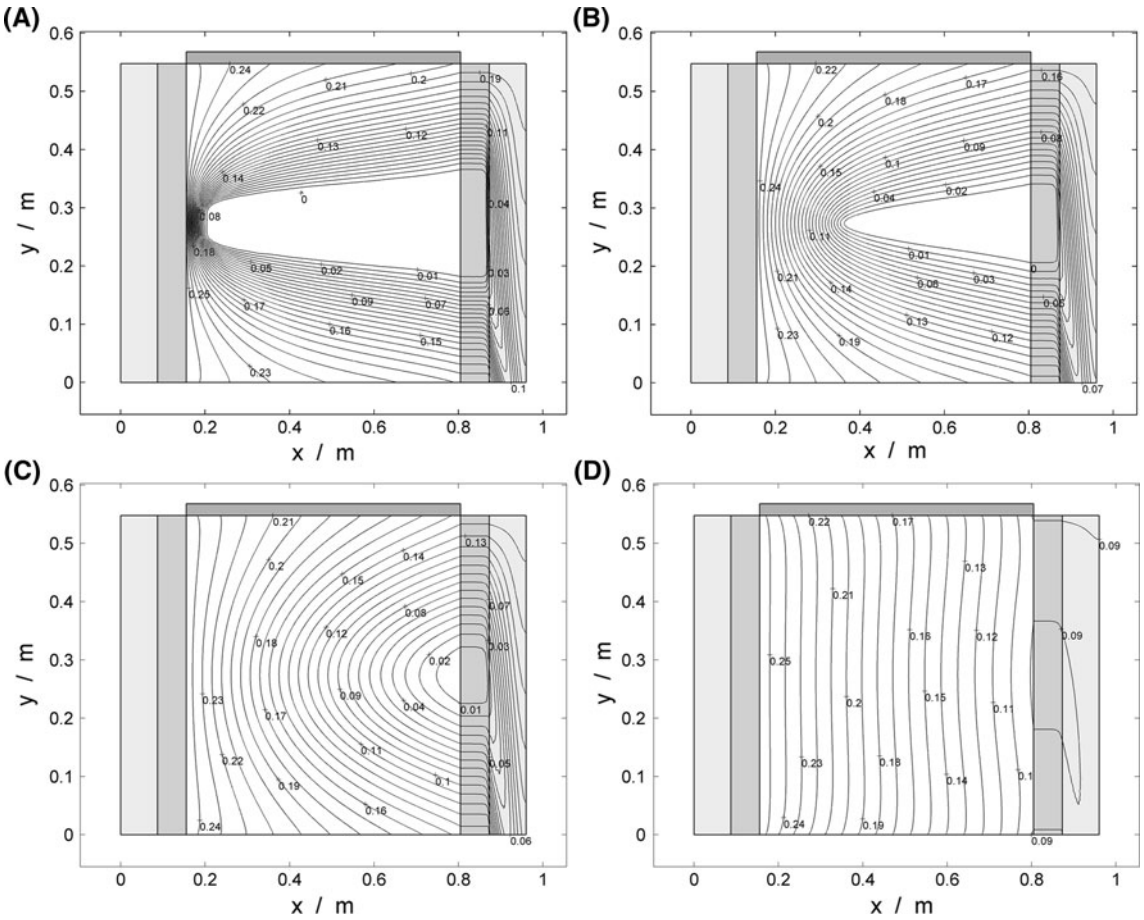

Fig. 10 Distribution of NaCl concentration in the diluate stream for different uniformity of the diluate and concentrate solution hydrodynamics, concentrations in (mol dm^{-3}); **A** extremely non-uniform hydrodynamics $\kappa_{15y} = 0.03$, GDD = 49 %, $U = 1710$ V, $U_p = 8.6$ V. **B** $\kappa_{15y} = 0.06$, GDD = 59 %, $U = 1014$ V, $U_p = 5.1$ V. **C** $\kappa_{15y} = 0.1$, GDD = 65 %, $U = 684$ V, $U_p = 3.4$ V. **D** uniform hydrodynamics $\kappa_{15y} = 1$, GDD = 64 %, $U = 653$ V, $U_p = 3.3$ V; remaining operational parameters: $I = 200$ A ($j_{in} = 961.5$ A m^{-2}), $Q = 8$ m^3 h^{-1}, $\bar{v}_{real} = 0.043$ m s^{-1}, $\Delta p = 40$ through 375 kPa, $c_{in} = 0.257$ mol dm^{-3}

this parameter in the next step. Flow irregularities are introduced into the model by decreasing the hydraulic permeability of the feed and drain channels (subdomains 1 and 5) in the *y*-direction. For this purpose a dimensionless permeability coefficient κ_{15y} was introduced into Eq. (19), used to evaluate $P_{1,y}$ and $P_{5,y}$. This finally leads to Eq. (21).

$$P_{1,y} = P_{5,y} = \kappa_{15y}\kappa_B B f_{1,C} = \kappa_{15y}\kappa_B B f_{1,D} \quad (21)$$

Parameter κ_{15y} is varied in a range from 1 (uniform hydrodynamics, results presented up to this point), through 0.1 and 0.06 down to $\kappa_{15y} = 0.03$. As it follows from Eq. (21), changes in κ_{15y} value results in artificial changes in the pressure drop on the ED stack calculated by the model. The corresponding distributions of the relative linear velocity in the working chambers related to the mean velocity are shown in Fig. 9A. The velocity profile corresponding to $\kappa_{15y} = 0.03$ is extremely non-uniform. Under these conditions the process solution is almost stagnant in the central compartments. Such a situation can hardly occur if the ED unit is constructed with sufficient precision and operated correctly. This parametric study aims to document the capability of the model and to study the situation of a possible malfunction of the membrane stack. In such a case it can be expected that the behaviour of the ED unit would be very close to the situation presented here.

The impact of the hydrodynamic non-uniformity on the *U–I* characteristic of the ED unit and the GDD is shown in Fig. 9B and C, respectively. In the case of uniform hydrodynamics (curve 4, $\kappa_{15y} = 1$), the *U–I* and GDD–*I* functions predicted by the proposed model are linear up to GDD = 80 %. A subsequent increase in non-uniformity, i.e. a reduction in the value of parameter κ_{15y}, leads to the occurrence of limiting current. This was evaluated by the model as approx. $I_{lim} = 220$ A for $\kappa_{15y} = 0.1$ (curve 3) and $I_{lim} = 90$ A, corresponding to $\kappa_{15y} = 0.03$ (curve 1). At current loads higher than the limiting value, the total voltage also increases linearly, but with a steeper slope. In the overlimiting current region its value is similar for all

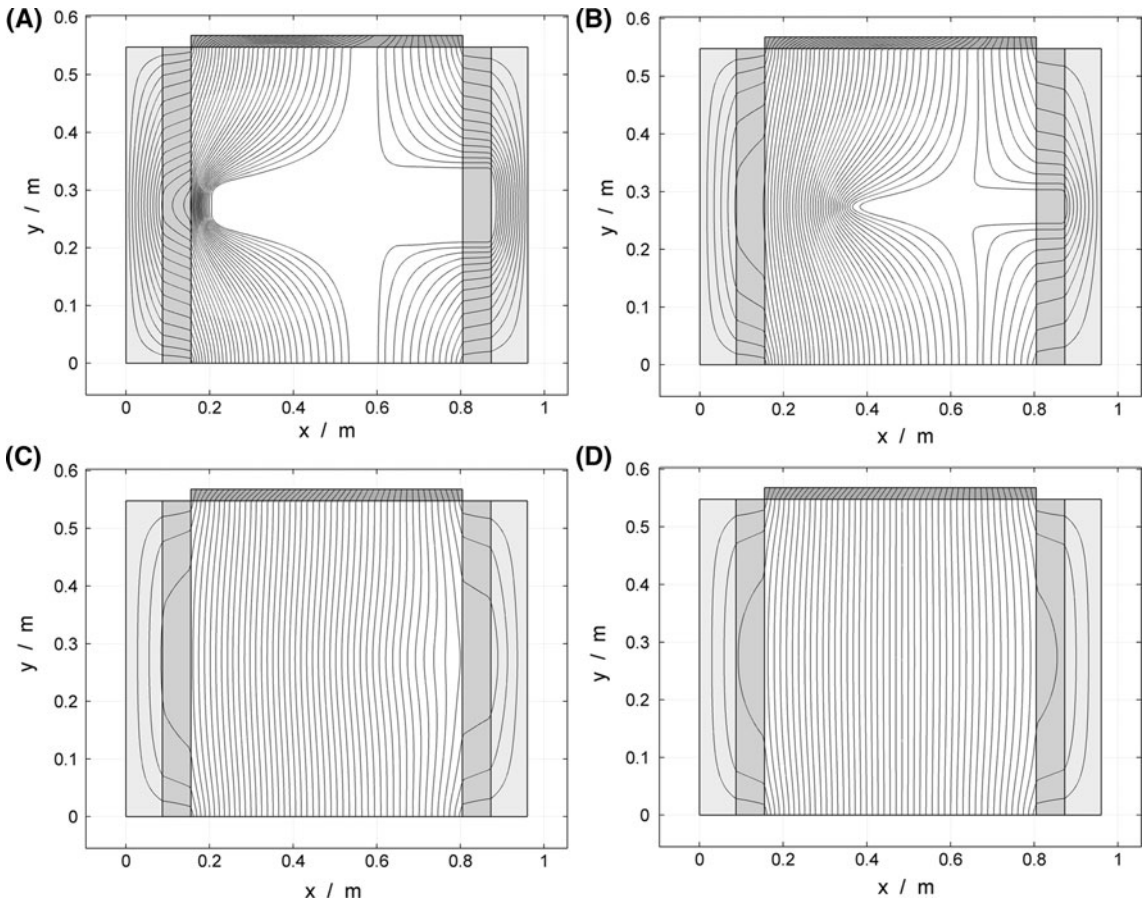

Fig. 11 Electric current lines in the ED unit for different uniformity of the diluate and concentrate solution hydrodynamics; **A** extremely non-uniform hydrodynamics $\kappa_{15y} = 0.03$, GDD = 49 %, $U = 1710$ V, $U_p = 8.6$ V, **B** $\kappa_{15y} = 0.06$, GDD = 59 %, $U = 1014$ V, $U_p = 5.1$ V, **C** $\kappa_{15y} = 0.1$, GDD = 65 %, $U = 684$ V, $U_p = 3.4$ V, **D** uniform hydrodynamics $\kappa_{15y} = 1$, GDD = 64.5 %, $U = 653$ V, $U_p = 3.3$ V; remaining operational parameters: $I = 200$ A ($j_{in} = 961.5$ A m^{-2}), $Q = 8$ m^3 h^{-1}, $\bar{v}_{real} = 0.043$ m s^{-1}, $\Delta p = 40$ through 375 kPa, $c_{in} = 0.257$ mol dm^{-3}

the studied values of parameters κ_{15y}. By contrast, in the overlimiting current region the GDD value increases with a significantly lower slope, indicating a significant loss of current efficiency. The explanation for all these aspects is clear from the local distribution of concentration and electric current lines discussed below. The impact of the flow non-uniformity on the required electric energy input P necessary to obtain the required degree of water desalination is shown in Fig. 9D. In this case the impact of flow uniformity is even more pronounced than it was on the U–I and GDD–I dependencies. The required electric energy input significantly increases in the overlimiting current region. As a result, the P needed for GDD = 40 % is almost three times higher in the case of extremely non-uniform distribution of v_D or v_C compared to uniform solution distribution. This difference then increases non-linearly with a further increase in GDD.

The local NaCl concentration field in a diluate stream is presented for $I = 200$ A in Fig. 10. It is evident that increasing flow non-uniformity causes a significant difference in the rate of desalination in the individual diluate compartments. In an extreme case, see Fig. 10A, the concentration decreases only slightly in the diluate compartments in the vicinity of the electrodes due to the very high linear velocity of the solution there. By contrast, the solution in the centre of the membrane stack is almost stagnant, which leads to a very rapid decrease in NaCl concentration to zero value directly behind the inlet to the working chamber. For this reason, the remaining part of the working chambers has almost zero NaCl concentration, rendering it almost electrically non-conductive. This results in the formation of significant inhomogeneity in the distribution of the current lines which are concentrated close to the inlet to the diluate chambers in the stack centre. This finally brings about a significant increase in the resistance of the membrane stack and in the slope of the U–I curve, see Fig. 9B. This resistance is proportional to the extent of the zone with zero NaCl concentration which grows

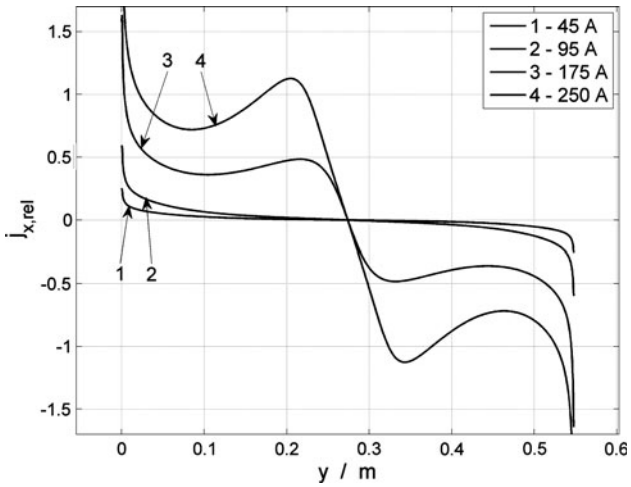

Fig. 12 Dependence of value of x-component of current density vector (j_x) along the boundary 7 (interface between inlet distribution channels and working chambers); values of j_x plotted in dimensionless form j_x divided by j_{in} (average current density at the anode feeder); non-uniform hydrodynamics $\kappa_{15y} = 0.03$; different current loads: (*1*) $I = 45$ A ($j_{in} = 216.5$ A m^{-2}, GDD = 14.5 %, $U = 141$ V, $U_p = 0.7$ V), (*2*) $I = 95$ A ($j_{in} = 456.5$ A m^{-2}, GDD = 30 %, $U = 340$ V, $U_p = 1.7$ V), (*3*) $I = 175$ A ($j_{in} = 841.5$ A m^{-2}, GDD = 45 %, $U = 1346$ V, $U_p = 6.7$ V), (*4*) $I = 250$ A ($j_{in} = 1202$ A m^{-2}, GDD = 56.5 %, $U = 2506$ V, $U_p = 12.5$ V); remaining operational parameters: $Q = 8$ m^3 h^{-1}, $\bar{v}_{real} = 0.043$ m s^{-1}, $\Delta p = 375$ kPa, $c_{in} = 0.257$ mol dm^{-3}

linearly with growing current load. This explains the linear constant slope of U–I in the overlimiting current region, shown in Fig. 9B.

The combination of significantly locally increased current density with low linear velocity in the entrance region of the working chambers in the centre of the stack can thus lead to an enormous rise in local temperature and a subsequent deterioration of the membranes. Such a situation, therefore, becomes highly dangerous in terms of process reliability. Another consequence of the non-uniform flow is the increase in parasitic current in the feed and drain channels in the position of the electrically insulating compartments due to low NaCl concentration, see Fig. 11. This finally leads to a loss of overall current efficiency of the ED process, as already mentioned in connection with Fig. 9C.

The influence of flow non-uniformity on the parasitic current flowing from the working chambers to the drain and feed channels can be easily evaluated from the dependence of the x-direction component of the local current density along the interface with the inlet distribution channels. The dependence of $j_{x,rel} = j_x/j_{in}$ along this interface, corresponding to $\kappa_{15y} = 0.03$ (extremely non-uniform hydrodynamics), is presented in Fig. 12. Two additional maxima appear on this dependency (compared to uniform flow hydrodynamics, see Fig. 8) in the central region of the ED unit (at $y = 0.21$ and 0.32 m) at a current load higher than the limiting value. These peaks indicate an increase in interfacial current flow and also, therefore, in the parasitic current value through the central region of the ED unit. Note also that the peak values of $j_{x,rel}$ increase with current load. Consequently, the parasitic current value increases as well and the overall current efficiency declines.

6 Conclusions

A novel macrohomogeneous mathematical modelling concept is proposed, enabling a calculation of the local distribution of various physical parameters, in this particular case concentrations and Galvani potential, in systems of complex geometry with periodically repeated parts. The example of a 2D model of an industrial-scale ED unit documents the viability of this approach. The computational demands of the proposed model are acceptable, while at the same time the model exhibits satisfactory accuracy and is, therefore, suitable for practical engineering calculations. The deviations between the model results and the experimental data observed in the present study arose due to the underestimated resistance of the membrane stack. This is a typical observation for this type of model of the ED process, caused by the simplification of the model physics. A linear correction of the model suffices to provide realistic results up to a medium degree of desalination. In the next step, a 3D model of an identical ED unit is needed to verify this explanation and to evaluate the impact of the model geometry simplifications on the accuracy of the results.

The capability of the model was verified by a parametric study of the impact of the inhomogeneity of the hydrodynamics of the process solution on the local distribution of concentration, Galvani potential and electric current lines in the ED unit. The model provided realistic results, permitting greater insight into the phenomena occurring in this type of process. It was proven that flow non-uniformity results in a significant decrease in overall process efficiency and significantly increases the risk of device failure due to local thermal deterioration of its components.

It should be noted that, although the proposed modelling concept was demonstrated on the example of an ED unit, it is not strictly limited to this process. It can be applied to a mathematical description of complex devices based on a plate-and-frame arrangement using membranes (reverse electrodialysis, fuel cells, membrane electrolysis, electrodeionization, membrane filtrations, etc.) or on other non-membrane systems.

Acknowledgments The authors gratefully acknowledge the financial support of this research by the Ministry of Industry and Trade of the Czech Republic within Project No. FR-TI1/479.

References

1. Strathmann H, Giorno L, Drioli E (2006) An introduction to membrane science and technology. Institute on Membrane Technology, CNR-ITM, Italy
2. Baker RW (2004) Membrane technology and applications, 2nd edn. Wiley, New York
3. Strathmann H (1991) Electrodialysis. In: Baker RW (ed) Membrane separation systems: recent developments and further directions. Noyes Data Corp, Park Ridge
4. Strathmann H (2010) Electrodialysis, a mature technology with a multitude of new applications. Desalination 264(3):268–288
5. Katz WE (1979) The electrodialysis reversal process. Desalination 28:31–40
6. Xu T, Huang C (2008) Electrodialysis-based separation technologies: a critical review. AIChE J 54(12):3147–3159
7. Slesarenko VV (2003) Electrodialysis and reverse osmosis membrane plants at power stations. Desalination 158:303–311
8. Greiter M, Novalin S, Wendland M, Kulbe KD, Fischer J (2002) Desalination of whey by electrodialysis and ion exchange resins: analysis of both processes with regard to sustainability by calculating their cumulative energy demand. J Membr Sci 210: 91–102
9. Tanaka Y (2007) Ion exchange membranes fundamentals and applications, 1st edn. Elsevier, Amsterdam
10. Veerman J, Post JW, Saakes M, Metza SJ, Harmsenb GJ (2008) Reducing power losses caused by ionic shortcut currents in reverse electrodialysis stacks by a validated model. J Membr Sci 310:418–430
11. Kodým R, Šnita D, Bouzek K, Thonstad J (2007) Potential and current density distributions along a bipolar electrode. J Appl Electrochem 37:1303–1312
12. Křišťál J, Kodým R, Bouzek K, Jiřičný V, Hanika J (2011) Electrochemical microreactor design for alkoxylation reactions—2. Experiments and simulations. Ind Eng Chem Res 51:1515–1524
13. Choi JH, Moon SH (2003) Structural change of ion-exchange membrane surfaces under high electric fields and its effects on membrane properties. J Colloid Interface Sci 265:93–100
14. Müller V, Roušar I (1991) Mass transfer coefficient and pressure losses for membrane cell with spacers. Dechema-Monographs 123:331–345
15. Nikonenko VV, Pismenskaya ND, Belova EI, Sistat P, Huguet P, Pourcelly G, Larchet Ch (2010) Intensive current transfer in membrane systems: modelling, mechanisms and application in electrodialysis. Adv Colloid Interface Sci 160:101–123
16. Dirkse MH, van Loon WKP, Stigter JD, Post JW, Veerman J, Bot GPA (2008) Extending potential flow modelling of flat-sheet geometries as applied in membrane-based systems. J Membr Sci 325:537–545
17. Kostoglou M, Karabelas AJ (2009) On the fluid mechanics of spiral-wound membrane modules. Ind Eng Chem Res 48: 10025–10036
18. Kodým R, Vlasák F, Šnita D, Černín A, Bouzek K (2011) Spatially two-dimensional mathematical model of the flow hydrodynamics in a channel filled with a net-like spacer. J Membr Sci 368:171–183
19. Pánek P, Kodým R, Šnita D, Bouzek K (2011) Spatially-2D mathematical model of the flow hydrodynamics in the spacer filled channel—effect of inertial forces. In: 9th ESEE, June 20–23, Crete/Greece, Book of abstracts, p 106, Proceedings CD of full texts
20. Mandersloot WGB, Hicks RE (1966) Leakage currents in electrodialytic desalting and brine production. Desalination 1: 178–193
21. Shaposhnik VA, Kuzminykh VA, Grigorchuk OV, Vasil'eva VI (1997) Analytical model of laminar flow electrodialysis with ion-exchange membranes. J Membr Sci 133:27–37
22. Lee HJ, Sarfert F, Strathmann H, Moon SH (2002) Designing of an electrodialysis desalination plant. Desalination 142:267–286
23. Brauns E, De Wilde W, Van den Bosch B, Lens P, Pinoy L, Empsten M (2009) On the experimental verification of an electrodialysis simulation model for optimal stack configuration design through solver software. Desalination 249:1030–1038
24. Veerman J, Saakes M, Metz SJ, Harmsen GJ (2011) Reverse electrodialysis: a validated process model for design and optimization. Chem Eng J 166:256–268
25. Tanaka Y (2000) Current density distribution and limiting current density in ion-exchange membrane electrodialysis. J Membr Sci 173:179–190
26. Tanaka Y (2010) A computer simulation of feed and bleed ion exchange membrane electrodialysis for desalination of saline water. Desalination 254:99–107
27. Tanaka Y (2005) Limiting current density of an ion-exchange membrane and of an electrodialyzer. J Membr Sci 266:6–17
28. Pánek P, Kodým R, Šnita D, Bouzek K (2011) Mathematical model of a single electrodialysis cell. In: 9th ESEE, June 20–23, Crete/Greece, Book of abstracts, p 61, Proceedings CD of full texts
29. De Wane HJ, Hamer WJ (1969) Electrochemical data PART XII—Electrolytic conductivity of aqueous solutions of the sodium halides, National Bureau of Standards report, U.S. Department of Commerce, National Bureau of Standards, NBS Report no.: 9979
30. MEGA a.s., Division of electrodialysis technology, Stráž pod Ralskem, Czech Republic, http://www.mega.cz